EUROPEAN ORGANIZATION FOR NUCLEAR RESEARCH

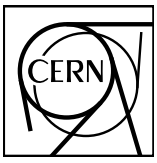

CERN-EP-2017-056
30 March 2017

J/ψ production as a function of charged-particle pseudorapidity density in p–Pb collisions at $\sqrt{s_{\rm NN}}$ = 5.02 TeV

ALICE Collaboration*

arXiv:1704.00274v1 [nucl-ex] 2 Apr 2017

Abstract

We report measurements of the inclusive J/ψ yield and average transverse momentum as a function of charged-particle pseudorapidity density $\mathrm{d}N_{\rm ch}/\mathrm{d}\eta$ in p–Pb collisions at $\sqrt{s_{\rm NN}}$ = 5.02 TeV with ALICE at the LHC. The observables are normalised to their corresponding averages in non-single diffractive events. An increase of the normalised J/ψ yield with normalised $\mathrm{d}N_{\rm ch}/\mathrm{d}\eta$ is observed at mid-rapidity and backward rapidity, similar to that found earlier in pp collisions. At forward rapidity, a saturation of the relative yield is observed for high charged-particle multiplicities. The normalised average transverse momentum at forward and backward rapidity increases with multiplicity at low multiplicities and saturates beyond moderate multiplicities. In addition, the forward-to-backward nuclear modification factor ratio is also reported, showing an increasing suppression of J/ψ production at forward rapidity with respect to backward rapidity for increasing charged-particle multiplicity.

© 2017 CERN for the benefit of the ALICE Collaboration.
Reproduction of this article or parts of it is allowed as specified in the CC-BY-4.0 license.

*See Appendix A for the list of collaboration members

1 Introduction

Quarkonium states, such as the J/ψ meson, are prominent probes of the deconfined state of matter, the Quark-Gluon Plasma (QGP), formed in high-energy heavy-ion collisions [1]. A suppression of bulk J/ψ production in nucleus-nucleus (AA) collisions with respect to that in proton-proton (pp) collisions has been observed by several experiments [2–10]. A remarkable feature is that, for J/ψ production at low transverse momentum ($p_{\rm T}$) at the Large Hadron Collider (LHC) the suppression is significantly smaller than at lower energies [5, 7, 10]. The measurements of J/ψ production in proton (deuteron)-nucleus collisions, where the formation of the QGP is not expected, are essential to quantify effects (often denominated "cold nuclear matter effects"), present also in AA collisions but not associated to the QGP formation. At LHC energies, gluon shadowing/saturation is the most relevant effect which was expected to be quantified with data in p–Pb collisions [11, 12]. Furthermore, a novel effect, coherent energy loss in cold nuclear matter (medium-induced gluon radiation), was proposed [13].

The measurements in d–Au collisions at the Relativistic Heavy Ion Collider (RHIC) have underlined the role of cold nuclear matter effects in J/ψ production at $\sqrt{s_{\rm NN}} = 200$ GeV [14–16]. At the LHC, the first measurements of J/ψ production in minimum-bias p–Pb collisions at $\sqrt{s_{\rm NN}} = 5.02$ TeV [17, 18] showed that J/ψ production in p–Pb collisions cannot be described by a simple superposition of nucleon-nucleon collisions. The data have been further analysed to provide more differential measurements and discussed in comparison with several theoretical models [19]. A fair agreement between data and models including nuclear shadowing [12] or saturation [20, 21] and models including a contribution from coherent energy loss in cold nuclear matter [13] is observed. These measurements are also relevant with respect to J/ψ production in Pb–Pb collisions at the LHC [5, 7], currently understood to be strongly influenced by the presence of a deconfined medium. The measurements of Υ production in minimum-bias p–Pb collisions at the LHC [22, 23] are also consistent with predictions based on cold nuclear matter effects. Recent measurements of the ψ(2S) state in p–Pb collisions have revealed a larger suppression than that measured for J/ψ production [24, 25]. Such an observation was not expected from the available predictions based on cold nuclear matter effects.

Concurrently, measurements of two-particle angular correlations in p–Pb collisions at the LHC [26–32] revealed for high-multiplicity events features that, in Pb–Pb collisions, have been interpreted as a result of the collective expansion of a hot and dense medium. Furthermore, the identified particle $p_{\rm T}$ spectra [33] show features akin to those in Pb–Pb collisions, where models including collective flow, assuming local thermal equilibrium, agree with the data.

The measurement of J/ψ production as a function of centrality in p–Pb collisions at the LHC [34] showed that the nuclear effects depend on centrality. Υ production has been studied as a function of charged-particle multiplicity in pp and p–Pb collisions by the CMS collaboration [35]. The yields of Υ mesons increase with multiplicity, while a decrease of the relative production of Υ(2S) and Υ(3S) with respect to Υ(1S) is observed. The measurement of D-meson production as a function of event multiplicity in p–Pb collisions [36] exhibits features similar to those observed earlier in pp collisions, both for J/ψ [37] and D-meson [38] production.

In this Letter measurements of the inclusive J/ψ yield and average transverse momentum as a function of charged-particle pseudorapidity density in p–Pb collisions at $\sqrt{s_{\rm NN}} = 5.02$ TeV are presented. Performed in three ranges of rapidity for $p_{\rm T} > 0$ with the ALICE detector at the LHC, these measurements complement the studies of J/ψ and $\psi(2S)$ production as a function of the event centrality estimated from the energy deposited in the Zero Degree Calorimeters (ZDC) [34, 39]. A measurement as a function of the charged particle multiplicity does not require an interpretation of the event quantiles in terms of the collision geometry. Importantly, it enables the possibility to study rare events where collective-like effects may arise. The present data allow the investigation of events with very high multiplicity of charged particles, corresponding to less than 1% of the hadronic cross section and establish as well a connection to

the recent measurements of D-meson production as a function of event multiplicity [36]. A measurement of the forward-to-backward J/ψ nuclear modification factor ratio is also presented.

2 Experiment and data sample

The ALICE central barrel detectors are located in a solenoidal magnetic field of 0.5 T. The main tracking devices in this region are the Inner Tracking System (ITS), which consists of six layers of silicon detectors around the beam pipe, and the Time Projection Chamber (TPC), a large cylindrical gaseous detector providing tracking and particle identification via specific energy loss. Tracks are reconstructed in the active volume of the TPC within the pseudorapidity range $|\eta| < 0.9$ in the laboratory frame. The first two layers of the ITS ($|\eta| < 2.0$ and $|\eta| < 1.4$), the Silicon Pixel Detector (SPD), are used for the collision vertex determination and the charged-particle multiplicity measurement. The minimum-bias (MB) events were triggered requiring the coincidence of the two V0 scintillator arrays covering $2.8 < \eta < 5.1$ and $-3.7 < \eta < -1.7$, respectively. The two neutron Zero Degree Calorimeters (ZDC), placed at 112.5 m on both sides of the interaction point, are used to reject electromagnetic interactions and beam-induced background. The muon spectrometer, covering $-4 < \eta < -2.5$, consists of a front absorber, a 3 T $\cdot$ m dipole magnet, ten tracking layers, and four trigger layers located behind an iron-wall filter. In addition to the MB trigger condition, the dimuon trigger requires the presence of two opposite-sign particles in the muon trigger chambers. The trigger comprises a minimum transverse momentum requirement of $p_{\rm T} >$0.5 GeV/c at track level. The trigger threshold is not sharp, and the single muon trigger efficiency plateau value ($\sim$ 96%) is reached at $p_{\rm T} \sim$ 1.5 GeV/c. The ALICE detector is described in more detail in [40] and its performance is outlined in [41].

The results presented in this Letter are obtained with data recorded in 2013 in p–Pb collisions at $\sqrt{s_{\rm NN}}$= 5.02 TeV. MB events are used for the J/ψ reconstruction in the dielectron channel at mid-rapidity. The dimuon-triggered data have been taken with two beam configurations, allowing the coverage of both forward and backward rapidity ranges. In the period when the dimuon-triggered data sample was collected, the MB interaction rate reached a maximum of 200 kHz, corresponding to a maximum pile-up probability of about 3%. The MB-triggered events used for the dielectron channel analysis were collected in one of the beam configurations at a lower interaction rate (about 10 kHz) and consequently had a smaller fraction of pile-up events of 0.2%.

Due to the asymmetry of the beam energy per nucleon in p–Pb collisions at the LHC, the nucleon-nucleon center-of-mass rapidity frame is shifted by $\Delta y = 0.465$ with respect to the laboratory system in the direction of the proton beam. This leads to a rapidity coverage in the nucleon-nucleon center-of-mass system $-1.37 < y_{\rm cms} < 0.43$ for the MB events, while the coverage for the dimuon-triggered data for the two different beam configurations is $-4.46 < y_{\rm cms} < -2.96$ (muon spectrometer located in the Pb-going direction) and $2.03 < y_{\rm cms} < 3.53$ (muon spectrometer located in the p-going direction). The integrated luminosities used in this analysis are 51.4$\pm$1.9 μb^{-1} (mid-rapidity), 5.01$\pm$0.19 nb^{-1} (forward y) and 5.81$\pm$0.20 nb^{-1} (backward y).

3 Charged-particle pseudorapidity density measurement

The charged-particle pseudorapidity density $\mathrm{d}N_{\rm ch}/\mathrm{d}\eta$ measurement is based on the SPD information. Tracklets, i.e. track segments built from hit pairs in the two SPD layers, were used together with the interaction vertex position, which was also determined with the SPD information [42]. Several quality criteria were applied to select only events with an accurate determination of the z coordinate of the vertex, $z_{\rm vtx}$. To ensure full SPD acceptance for the tracklet multiplicity $N_{\rm trk}$ evaluation within $|\eta| < 1$, the condition $|z_{\rm vtx}| < 10$ cm was applied for the selection of the events.

During the data taking period about 8% of the SPD channels were inactive, the exact fraction being

time-dependent. The impact of the inactive channels of the SPD on the tracklet multiplicity measurement varies with $z_{\rm vtx}$. A $z_{\rm vtx}$-dependent correction factor was determined from data, as discussed in [37]. The correction factor was randomised on an event-by-event basis using a Poisson distribution in order to emulate the dispersion between the true charged-particle multiplicity and the measured tracklet multiplicities.

The overall inefficiency, the production of secondary particles due to interactions in the detector material, particle decays and fake-tracklet reconstruction lead to a difference between the number of reconstructed tracklets and the true primary charged-particle multiplicity $N_{\rm ch}$ (see details in [42])[1]. Using events simulated with the DPMJET event generator [43], the correlation between the tracklet multiplicity (after the $z_{\rm vtx}$-correction), $N_{\rm trk}^{\rm corr}$, and the generated primary charged particles $N_{\rm ch}$ was determined. The correction factor β to obtain the average $\mathrm{d}N_{\rm ch}/\mathrm{d}\eta$ value corresponding to a given $N_{\rm trk}^{\rm corr}$ bin was computed from a linear fit of the $N_{\rm trk}^{\rm corr}$- $N_{\rm ch}$ correlation. The charged-particle pseudorapidity density value in each multiplicity bin is given relative to the event-averaged value and was calculated as: $\mathrm{d}N_{\rm ch}^{R}/\mathrm{d}\eta = \mathrm{d}N_{\rm ch}/\mathrm{d}\eta / \langle \mathrm{d}N_{\rm ch}/\mathrm{d}\eta \rangle = \beta \cdot \langle N_{\rm trk}^{\rm corr} \rangle / \left(\Delta\eta \cdot \langle \mathrm{d}N_{\rm ch}/\mathrm{d}\eta \rangle\right)$, where $\Delta\eta = 2$ and $\langle \mathrm{d}N_{\rm ch}/\mathrm{d}\eta \rangle$ is the charged-particle pseudorapidity density for non-single diffractive (NSD) collisions, which was measured to be $\langle \mathrm{d}N_{\rm ch}/\mathrm{d}\eta \rangle = 17.64 \pm 0.01(\mathrm{stat.}) \pm 0.15(\mathrm{syst.})$ [42]. The resulting values for the multiplicity bins are summarised in Tables 1 and 2 for forward and mid-rapidity, respectively. For the data at backward rapidity, the values are very close to those at forward rapidity.

$\mathrm{d}N_{\rm ch}/\mathrm{d}\eta$	$\mathrm{d}N_{\rm ch}^{R}/\mathrm{d}\eta$	σ/σ_{MB}
4.8 ± 0.2	0.27 ± 0.01	26.4%
10.9 ± 0.4	0.62 ± 0.03	14.3%
14.6 ± 0.5	0.83 ± 0.03	7.9%
17.8 ± 0.5	1.01 ± 0.04	9.6%
21.4 ± 0.7	1.22 ± 0.05	8.5%
25.0 ± 0.8	1.42 ± 0.06	7.2%
28.6 ± 0.8	1.62 ± 0.06	6.0%
32.7 ± 1.0	1.85 ± 0.07	6.7%
37.8 ± 1.1	2.14 ± 0.08	4.6%
44.2 ± 1.3	2.51 ± 0.10	4.2%
54.3 ± 1.6	3.08 ± 0.12	2.4%
71.4 ± 2.1	4.05 ± 0.16	0.3%

Table 1: Average charged-particle pseudorapidity density values (absolute and relative) in each multiplicity bin, obtained from $N_{\rm trk}^{\rm corr}$ measured in the range $|\eta| < 1$. The values correspond to the data sample used for the forward rapidity analysis. Only systematic uncertainties are shown since the statistical ones are negligible. The fraction of the MB cross section for each multiplicity bin is also indicated.

$\mathrm{d}N_{\rm ch}/\mathrm{d}\eta$	$\mathrm{d}N_{\rm ch}^{R}/\mathrm{d}\eta$	σ/σ_{MB}
6.9 ± 0.2	0.39 ± 0.02	47.2%
22.9 ± 0.6	1.30 ± 0.05	39.7%
42.3 ± 1.1	2.40 ± 0.10	10.9%
64.4 ± 1.6	3.65 ± 0.15	1.0%

Table 2: As Table 1, but for the analysis of J/ψ production at mid-rapidity.

The fraction of the MB cross section contained in each multiplicity bin (σ/σ_{MB}, derived from the respective event counts in the multiplicity bins and total number of MB events) is reported in Tables 1 and

[1] In this context, we regard as primary charged-particles all prompt charged particles including all decay products except products from weak decays of light flavour hadrons and of muons.

2. The softest MB events, which lead to absence of tracklets in $|\eta| < 1$ are not accounted for in this analysis. They correspond to 1.2% of σ_{MB} for the MB-triggered events and 1.9% for the muon-triggered data; the difference is due to the different fraction of inactive channels in SPD and affects, albeit in a negligible way, only our first multiplicity bin.

The multiplicity selection in this analysis allowed to sample the data in bins containing a small fraction of the MB cross section. Therefore, it gives the possibility to study the J/ψ production in rare high-multiplicity events which were not accessible in the centrality-based analysis [34] (where the most-central event class corresponds to the range 2-10% in σ/σ_{MB}).

4 J/ψ measurement

For the J/ψ analysis at forward and backward rapidities, muon candidates were selected by requiring the reconstructed track in the muon chambers to match a track segment in the trigger chambers. Furthermore, the radial distance of the muon tracks with respect to the beam axis at the end of the front absorber was required to be between 17.6 and 89.5 cm. This criterion rejects tracks crossing the high-density part of the absorber, where the scattering and energy-loss effects are large. A selection on the muon pseudorapidity $-4 < \eta < -2.5$ was also applied to reject muons at the edges of the spectrometer's acceptance.

When building the invariant mass distributions, each dimuon pair (of a given $p_{\rm T}$ and y) was corrected by the detector acceptance times efficiency factor $1/(A\times\varepsilon(p_{\rm T},y))$. The $A\times\varepsilon(p_{\rm T},y)$ map was obtained from a particle-gun Monte Carlo simulation based on GEANT 3 [44] and simulating the detector response as in [18]. Since the $A\times\varepsilon$-factor does not depend on the multiplicity for the event multiplicities relevant for the p–Pb analyses, the simulated events only contain a dimuon pair at the generator level. The simulations assume an unpolarised J/ψ production. The extraction of the J/ψ signal in the dimuon channel was performed via a fit to the $A\times\varepsilon$-corrected opposite-sign (OS) dimuon invariant mass distributions obtained for $p_{\rm T} < 15$ GeV/c (Fig. 1). The fitting procedure is equivalent to that used in a previous J/ψ analysis in p–Pb collisions [18]. The distributions were fitted using a superposition of J/ψ and ψ(2S)signals and a background shape. The resonances are parametrised using a Crystal Ball function with asymmetric tails or a pseudo-Gaussian function, while for the background a polynomial times exponential function or a Gaussian with a width linearly varying with mass are used. In the present analysis, the parameters of the non-Gaussian tails of the resonance shapes were tuned on the Monte Carlo J/ψ signal.

In the dielectron decay channel, electrons and positrons were reconstructed in the central barrel detectors by requiring a minimum of 70 out of maximally 159 track points in the TPC and a value of the track fit χ^2 over the number of track points smaller than 4 were required. Furthermore, only tracks with at least two associated hits in the ITS, one of them in the innermost layer, were accepted. This selection reduced the amount of electrons and positrons from photon conversions in the material of the detector beyond the first ITS layer. In addition a veto cut on topologically identified tracks from photon conversions was applied. The electron identification was achieved by the measurement of the energy deposition of the track in the TPC, which was required to be compatible with that expected for electrons within 3 standard deviations. Tracks with specific energy loss being consistent with that of the pion or proton hypothesis within 3.5 standard deviations were rejected. These selection criteria are identical to those used in [34]. Electrons and positrons were selected in the pseudorapidity range $|\eta| < 0.9$ and in the transverse momentum range $p_{\rm T} > 1$ GeV.

The background in the OS invariant mass distribution was estimated with dielectron pairs formed with tracks from different events (mixed-event background). The background shape was normalised such that its integral over ranges of the invariant mass in the sidebands of the J/ψ mass peak equals the number of measured OS dielectron pairs in the same ranges (typical ranges used are $[3.2, 3.7]$ GeV/c^2 and $[2.0, 2.5]$ GeV/c^2). The signal itself was extracted by counting the entries in the background-subtracted invariant mass distribution (the standard range used is $[2.92, 3.16]$ GeV/c^2). Due to bremsstrahlung of the electron

and positron in the detector material and radiative corrections of the decay vertex, the J/ψ signal shape has a tail towards lower invariant masses. The standard range for the signal extraction contains, according to Monte Carlo simulations, about 69% of the J/ψ signal. The number of reconstructed J/ψ is defined as the mean obtained when varying the counting window for the signal extraction and the invariant mass ranges used for the normalisation of the background. The variations that were taken into account are the same as in [34].

The correction for the acceptance and efficiency of the raw yields is based on simulated p–Pb collisions with the HIJING event generator [45] with an injected J/ψ signal. The dielectron decay is simulated with the EVTGEN package [46] using PHOTOS [47, 48] to describe the final state radiation. The production is assumed to be unpolarised as in the muon decay channel analysis. The propagation of the simulated particles is done by GEANT 3 [44] and a full simulation of the detector response is performed. The same reconstruction procedure and selection cuts are applied to MC events and to real data.

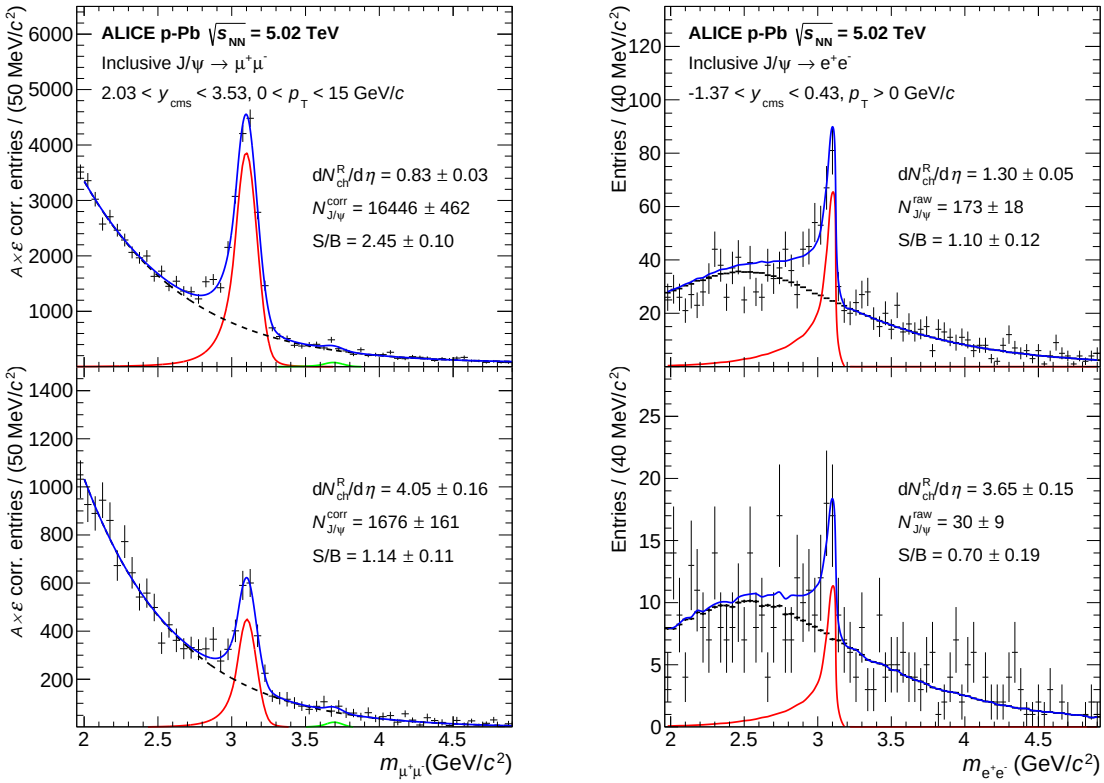
ALICE p-Pb $\sqrt{s_{NN}}$ = 5.02 TeV
Inclusive J/ψ → μ⁺μ⁻
2.03 < y_{cms} < 3.53, 0 < p_T < 15 GeV/c
$dN^R_{ch}/d\eta$ = 0.83 ± 0.03
$N^{corr}_{J/\psi}$ = 16446 ± 462
S/B = 2.45 ± 0.10
$dN^R_{ch}/d\eta$ = 4.05 ± 0.16
$N^{corr}_{J/\psi}$ = 1676 ± 161
S/B = 1.14 ± 0.11
A×ε corr. entries / (50 MeV/c²)
$m_{\mu^+\mu^-}$(GeV/c²)
ALICE p-Pb $\sqrt{s_{NN}}$ = 5.02 TeV
Inclusive J/ψ → e⁺e⁻
-1.37 < y_{cms} < 0.43, p_T > 0 GeV/c
$dN^R_{ch}/d\eta$ = 1.30 ± 0.05
$N^{raw}_{J/\psi}$ = 173 ± 18
S/B = 1.10 ± 0.12
$dN^R_{ch}/d\eta$ = 3.65 ± 0.15
$N^{raw}_{J/\psi}$ = 30 ± 9
S/B = 0.70 ± 0.19
Entries / (40 MeV/c²)
$m_{e^+e^-}$ (GeV/c²)

Fig. 1: Opposite-sign invariant mass distributions of selected muon (left panel, for the forward rapidity) and electron (right panel) pairs, for selected multiplicity bins. In the left panel, the distributions are corrected for $A\times\varepsilon$. The curves show the fit functions for signal, background and combined signal and background (see text for details). In the right panel, the background is evaluated with the event-mixing technique, the overlaid signal is obtained from Monte Carlo (see text for details).

The inclusive J/ψ yield was obtained in each multiplicity bin as $N_{J/\psi} = N^{corr}_{J/\psi}/N_{MB}$, where $N^{corr}_{J/\psi}$ is the number of reconstructed J/ψ corrected for the acceptance times efficiency factor. In the dimuon decay channel analysis, the number of MB events equivalent to the analysed dimuon sample (N_{MB}) in each multiplicity bin was obtained from the number of dimuon triggers (N_{DIMU}), through the normalisation factor of dimuon-triggered to MB-triggered events $F_{2\mu/MB}$, as $N_{MB} = F_{2\mu/MB} \cdot N_{DIMU}$. This factor was computed using two different methods, as discussed in [34]. The J/ψ cross section values for minimum-bias events obtained in the dimuon channel at forward and backward rapidity, and in the dielectron

channel at mid-rapidity are compatible with those presented in [18] and [19], respectively. The results presented here are provided relative to the yield in NSD events, $\langle \mathrm{d}N_{J/\psi}/\mathrm{d}y \rangle$. The event-averaged yield is normalised to the NSD event class; the normalisation uncertainty is 3.1% [42].

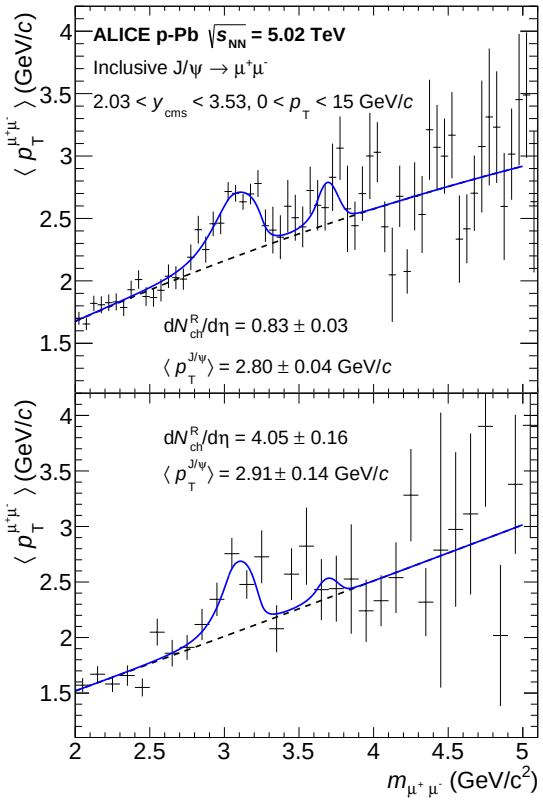
ALICE p-Pb $\sqrt{s_{NN}}$ = 5.02 TeV
Inclusive J/ψ → μ⁺μ⁻
2.03 < y_{cms} < 3.53, 0 < p_T < 15 GeV/c
$dN^R_{ch}/d\eta$ = 0.83 ± 0.03
$\langle p_T^{J/\psi} \rangle$ = 2.80 ± 0.04 GeV/c
$dN^R_{ch}/d\eta$ = 4.05 ± 0.16
$\langle p_T^{J/\psi} \rangle$ = 2.91± 0.14 GeV/c
$\langle p_T^{\mu^+\mu^-} \rangle$ (GeV/c)
$m_{\mu^+\mu^-}$ (GeV/c²)

Fig. 2: Average transverse momentum of opposite-sign muon pairs as a function of the invariant mass at forward rapidity, for two multiplicity bins. The curves are fits of the background and combined signal and background (see text).

In previous analyses, e.g. [19], the J/ψ yield was extracted in p_{T} bins, and the resulting distribution was fitted to extract the $\langle p_{\mathrm{T}} \rangle$ value. The present analysis aims at studying effects that may arise at high charged-particle multiplicities, where the usual method is no longer suitable due to statistical limitations. The method presented here does not require to sample the data in p_{T} bins, hence allowing the analysis in finer multiplicity bins. The extraction of the average transverse momentum of J/ψ mesons was done via a fit of the dimuon mean transverse momentum as a function of the invariant mass, $\langle p_{\mathrm{T}}^{\mu^+\mu^-} \rangle (m_{\mu^+\mu^-})$. A correction for the acceptance times efficiency has to be applied when building these distributions. Hence, the contribution of each dimuon pair with a certain p_{T} and y in a given invariant mass bin was weighted with the two-dimensional $A\times\varepsilon(p_{\mathrm{T}},y)$. In order to extract the J/ψ $\langle p_{\mathrm{T}} \rangle$, the $A\times\varepsilon$-corrected $\langle p_{\mathrm{T}}^{\mu^+\mu^-} \rangle (m_{\mu^+\mu^-})$ distributions, which are shown in Fig. 2, were fitted using the following functional shape:

$$\begin{aligned} \langle p_{\mathrm{T}}^{\mu^+\mu^-} \rangle (m_{\mu^+\mu^-}) &= \alpha^{J/\psi}(m_{\mu^+\mu^-}) \times \langle p_{\mathrm{T}}^{J/\psi} \rangle \\ &+ \alpha^{\psi(2S)}(m_{\mu^+\mu^-}) \times \langle p_{\mathrm{T}}^{\psi(2S)} \rangle \\ &+ \left(1 - \alpha^{J/\psi}(m_{\mu^+\mu^-}) - \alpha^{\psi(2S)}(m_{\mu^+\mu^-})\right) \times \langle p_{\mathrm{T}}^{\mathrm{bkg}} \rangle \end{aligned} \quad (1)$$

where $\alpha(m_{\mu^+\mu^-}) = S(m_{\mu^+\mu^-})/(S(m_{\mu^+\mu^-}) + B(m_{\mu^+\mu^-}))$; the signal ($S$) and background ($B$) dependence on the dimuon invariant mass was extracted from the corrected invariant mass spectrum fits mentioned

above. The J/ψ and ψ(2S) average transverse momentum, $\langle p_{\rm T}^{J/\psi}\rangle$ and $\langle p_{\rm T}^{\psi(2S)}\rangle$, are fit parameters, while the background one, $\langle p_{\rm T}^{\rm bkg}\rangle$, was parametrized with a second order polynomial function. Note that, as for the yield extraction, the quantity $\langle p_{\rm T}^{\psi(2S)}\rangle$ is not a measurement of the ψ(2S) mean transverse momentum, since the $A\times\varepsilon$ was obtained only from J/ψ signals in the simulation. The $\langle p_{\rm T}\rangle$ results presented here for bins in multiplicity are relative to the value obtained for inclusive events [19].

5 Systematic uncertainties

The systematic uncertainty of the overall average charged-particle pseudorapidity density was estimated to be 3.8% [42]. This includes effects related to the uncertainties in the simulations, detector acceptance and event selection efficiency, and it is dominated by the normalisation to the NSD event class. Possible correlation between the average multiplicity and that evaluated in a given bin would lead to a partial cancellation of certain sources of uncertainty when computing the relative multiplicity. As a conservative estimate, the uncertainty on the relative multiplicity was considered to be equal to the uncertainty on the overall charged-particle pseudorapidity density.

The influence of variations of the η distribution in the calculation of the β correction factors, was estimated from the difference between the average number of tracklets obtained in the data taken with the two different beam configurations. The corresponding uncertainty on the multiplicity determination amounts to 1%. The uncertainties arising from the fit procedure of the $N_{\rm trk}^{\rm corr}$- $N_{\rm ch}$ correlation in simulated events, used to obtain the correction factors, were also included as systematic uncertainty. This uncertainty ranges between 0.2% (at high multiplicity) and 2% (at low multiplicity). The event selection related to the vertex quality has a 1% effect on the average multiplicity in the lowest multiplicity bin and a negligible effect for the other bins. Due to the uncertainty on the determination of the multiplicity of the individual events, there could be a migration of events among the multiplicity bins (bin-flow). This bin-flow effect was determined by running the analysis several times with different seeds for the random factor of the multiplicity correction (bin-flow test). The bin-flow uncertainties were obtained from the dispersion of the average multiplicity values in the bin-flow tests for each multiplicity bin. Finally, the effect of pile-up was studied using a toy model that reproduces the main features of the multiplicity determination, and takes into account the mis-identification of multiple collisions in the same event. The contribution of bin-flow and pile-up to the measured multiplicities were found to be negligible for all the data sets (taken at different interaction rates). The bin-dependent uncertainty was added in quadrature to the 3.8% uncertainty of $\langle {\rm d}N_{\rm ch}/{\rm d}\eta\rangle$, resulting in a systematic uncertainty of the relative charged-particle multiplicity of $4-4.5$% depending on the multiplicity bin.

The yields reported here are provided relative to the event-average yield and the uncertainties were estimated for this ratio. The systematic uncertainties related to trigger, tracking and matching efficiency are correlated between the multiplicity-differential and the integrated determinations. They cancel out to a large extent.

In the dimuon analysis, a combined systematic uncertainty which includes the $A\times\varepsilon$ variations due to the uncertainty of the J/ψ $p_{\rm T}$ and rapidity input distributions used in the simulation and multiplicity bin-flow effects was derived. Due to the multiplicity bin-flow, and the fact that the invariant mass and $\langle p_{\rm T}^{\mu^+\mu^-}\rangle(m_{\mu^+\mu^-})$ spectra were weighted by $A\times\varepsilon$, these uncertainties could not be computed separately. The combined uncertainty was obtained from the r.m.s. of the relative yield values obtained running the analysis several times with different seeds for the random factor of the multiplicity correction. In addition the systematic uncertainty for the signal extraction was estimated as the r.m.s. of the results obtained using different fitting assumptions for a given bin-flow test. The uncertainty related to the computation method of the relative $F_{2\mu/MB}$ was estimated considering the difference between the two available methods to measure the factor in multiplicity bins [34]. The uncertainties due to the determination of the parameters of the signal tails and the effect of the vertex quality selection were also computed. Finally,

in order to determine the pile-up effect on the measured yield in each multiplicity bin, the pile-up toy model was extended by including the production of J/ψ using as input the measured yields. All these effects are uncorrelated within a given multiplicity bin, hence they were added quadratically to obtain the systematic uncertainty of the relative yield in a multiplicity bin. Also, these systematic uncertainties were considered as uncorrelated between the different rapidity intervals. A summary of the maximum and minimum relative yield systematic uncertainties is shown in Tab. 3. In addition, the 3.1% uncertainty of the event-average yield normalisation to NSD, is reported separately.

The systematic uncertainties were computed also for the absolute yields in multiplicity bins at forward and backward rapidity. The absolute yields were used to compute the ratio of the nuclear modification factors at forward and backward rapidities. The values of the uncertainties on the absolute yields are shown in parentheses in Tab. 3, when they are different from the ones obtained for the relative yield. In addition, for the absolute measurement the muon tracking, trigger and matching efficiency uncertainties were needed to be taken into account [18]. They amount to 4% (6%), 3% (3.4%) and 1% (1%) at forward (backward) rapidity respectively.

Source	$2.03 < y_{\rm cms} < 3.53$	$-4.46 < y_{\rm cms} < -2.96$	$-1.37 < y_{\rm cms} < 0.43$
Sig. Extr.	$0.6 - 1.9\%$	$0.5 - 1.8\%$	$3.2 - 8.4\%$
$F_{2\mu/MB}$ method	$0.3 - 3.9\%$	$0.3 - 3.9\%$	not applicable
$A\times\varepsilon$./bin-flow	$1 - 5.9\%$	$1.4 - 3.9\%$	$3.1 - 9.9\%$
Pile-up	$1 - 4\%$	$1 - 1.5\%$	negligible
Signal tails	0.5% (2%)	0.5% (2%)	not applicable
Vertex quality sel.	$0.6\,^{*} - 0.3\%$ ($0.9^{*}\%$)	$0.6^{*} - 0.3\%$ ($0.9^{*}\%$)	negligible
Total	$2.1 - 8.3\%$ ($3.0 - 8.6\%$)	$2.1 - 6.0\%$ ($2.9 - 6.4\%$)	$4.5 - 13\%$

Table 3: The systematic uncertainties of the relative J/ψ yield measurement in the three rapidity ranges. The values in parentheses correspond to the absolute yield measurement when different from the relative ones. The ranges represent the minimum and maximum values of the uncertainties over the multiplicity bins. The uncertainties marked with * refer only to the lowest-multiplicity bin. The trigger, tracking and matching efficiency uncertainties are not listed in the table.

For the dielectron decay channel, the signal extraction uncertainty was derived based on the r.m.s. value of the different signal yield ratios obtained for the variations of the background and the signal integration window as in [34]. The uncertainty is largest for the highest multiplicity bins. Since the $p_{\rm T}$ distribution of J/ψ may depend on multiplicity, the unmeasured $p_{\rm T}$ spectrum leads to a multiplicity-dependent uncertainty, determined as in [34]. As explained in section 2, the pile-up contamination is very low and the induced uncertainty is negligible for all the multiplicity intervals. The uncertainty related to bin-flow was estimated with the same method as in the dimuon analysis. The total systematic uncertainty varies as a function of multiplicity between 3.2% and 8.4%, see Tab. 3.

For the relative J/ψ $\langle p_{\rm T}\rangle$, the effects of the uncertainty on the determination of $A\times\varepsilon$, the $\langle p_{\rm T}\rangle$ extraction procedure and bin-flow were computed together following the same procedure as for the relative yield. The $\langle p_{\rm T}\rangle$ extraction uncertainty was obtained from the dispersion of the results using different fit combinations. The effect of considering the J/ψ $\langle p_{\rm T}\rangle$ as independent of the invariant mass in the $\langle p_{\rm T}^{\mu^+\mu^-}\rangle$ fits was negligible. The impact of fixing the signal and background parameters during the fitting procedure was observed to be negligible as well. Finally, using a pile-up toy model, it was shown that the pile-up had no effect on the $\langle p_{\rm T}\rangle$ measurement, except for the two bins corresponding to the largest multiplicities. All these effects were considered as uncorrelated in a given multiplicity bin and hence their respective uncertainties were added quadratically to obtain the relative $\langle p_{\rm T}\rangle$ systematic uncertainty in each multiplicity bin. These systematic uncertainties were considered as uncorrelated between the different rapidity intervals. The results of the uncertainties entering in the relative $\langle p_{\rm T}\rangle$ measurement are reported in Tab. 4.

Source	$2.03 < y_{\rm cms} < 3.53$	$-4.46 < y_{\rm cms} < -2.96$
Sig. extr.	$0.2 - 1.2\%$	$0.2 - 0.5\%$
$A\times\varepsilon$/bin-flow	$0.5 - 2.0\%$	$0.7 - 2.7\%$
Pile-up	$0.2 - 0.7\%^*$	$0.2 - 0.8\%^*$
Total	$0.6 - 2.4\%$	$0.7 - 2.9\%$

Table 4: The systematic uncertainties for the relative $\langle p_{\rm T}\rangle$ measurement at forward and backward rapidity. The values represent the minimum and maximum values of the uncertainties over the multiplicity bins. The uncertainties marked with * only refer to the two highest-multiplicity bins.

6 Results and discussion

The dependence of the relative J/ψ yield on the relative charged-particle pseudorapidity density for three J/ψ rapidity ranges is presented in Fig. 3. An increase of the relative yield with charged-particle multiplicity is observed for all rapidity domains, with a similar behaviour at low multiplicities. At multiplicities beyond $1.5-2$ times the event-average multiplicity, two different trends are observed. The relative yields at mid-rapidity and backward rapidity keep growing with the relative multiplicity in p–Pb collisions similarly to the observation in pp collisions at 7 TeV [37]. At forward rapidity the trend is different. In this rapidity window a saturation of the relative yield sets in for high multiplicities. In lack of theoretical model calculations, it is unclear at the moment what is the cause of this observation. We recall that the explored Bjorken x ranges in the forward rapidity region are in the domain of shadowing/saturation, and that a variety of models [12, 13, 20, 21, 49] are fairly successful in describing the recent centrality-integrated and differential measurements of ALICE [19, 34], which correspond in terms of our relative multiplicities to $\mathrm{d}N_{\rm ch}/\mathrm{d}\eta\,/\langle \mathrm{d}N_{\rm ch}/\mathrm{d}\eta\rangle \simeq 2.5$ at most.

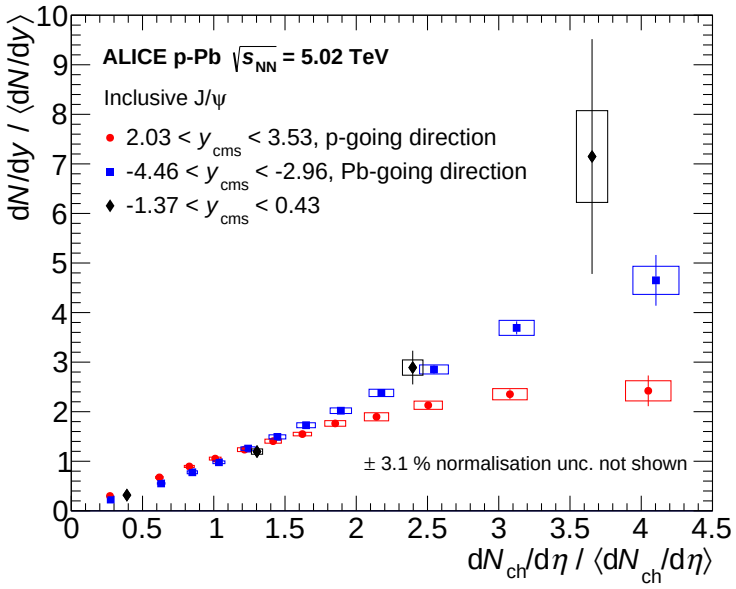

Fig. 3: Relative yield of inclusive J/ψ mesons as a function of relative charged-particle pseudorapidity density for three rapidity regions. The error bars show the statistical uncertainties, the boxes the systematic ones.

In Fig. 4 the J/ψ measurement at mid-rapidity is compared to that for prompt D mesons (average of D^0, D^+, and D^{*+} species) for the $p_{\rm T}$ range $2-4$ GeV/c [36]. Similar trends are seen for the J/ψ and D mesons, as observed earlier in pp collisions [38].

The nuclear modification factor for J/ψ production in p–Pb collisions ($R_{\rm pPb}$) as a function of centrality was presented in [34]. The relationship between geometry-related quantities, that quantify the centrality

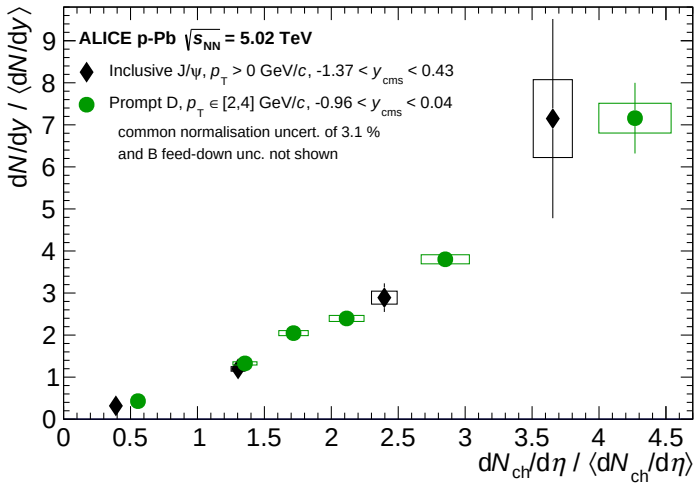
ALICE p-Pb $\sqrt{s_{NN}}$ = 5.02 TeV
Inclusive J/ψ, p_T > 0 GeV/c, -1.37 < y_{cms} < 0.43
Prompt D, p_T ∈ [2,4] GeV/c, -0.96 < y_{cms} < 0.04
common normalisation uncert. of 3.1 %
and B feed-down unc. not shown
dN/dy / ⟨dN/dy⟩
dN$_{ch}$/dη / ⟨dN$_{ch}$/dη⟩

Fig. 4: Relative yield of inclusive J/ψ mesons as a function of relative charged-particle pseudorapidity density in comparison to D mesons (average of D^0, D^+, and D^{*+} species), for the p_T interval 2-4 GeV/c [36]. The error bars show the statistical uncertainties, the boxes the systematic ones (for the D mesons, additional systematic uncertainties due to the b feed-down contributions and the event normalisation are not shown).

of the collision, and experimental observables in p–Pb collisions may be subject to a selection bias [50] which needs care in interpretation. By performing the ratio of the nuclear modification factors at forward and backward rapidities as a function of multiplicity, the dependence on geometry-related quantities is eluded. The forward-to-backward nuclear modification factor ratio is defined as:

$$\begin{aligned} R_{\rm FB} &= \frac{R_{\rm pPb}(2.03 < y_{\rm cms} < 3.53)}{R_{\rm pPb}(-4.46 < y_{\rm cms} < -2.96)} \\ &= \frac{Y^{J/\psi}_{\rm pPb}(2.03 < y_{\rm cms} < 3.53)}{Y^{J/\psi}_{\rm pPb}(-4.46 < y_{\rm cms} < -2.96)} \times \frac{{\rm d}\sigma^{J/\psi}_{\rm pp}/{\rm d}y(-4.46 < y_{\rm cms} < -2.96)}{{\rm d}\sigma^{J/\psi}_{\rm pp}/{\rm d}y(2.03 < y_{\rm cms} < 3.53)} \end{aligned} \quad (2)$$

Since the average charged-particle multiplicities and their uncertainties are very close to each other for the two sets of data, the values of $R_{\rm FB}$ are shown versus the average value of the two in each multiplicity bin. Note that, differently than for the case of the nuclear modification factor measurement in [18], for the present measurement the rapidity ranges are not symmetric with respect to $y_{\rm cms}$ = 0 to take advantage of all the signal yield, allowing the study up to high multiplicities. The values of the reference pp cross-section were obtained by means of an interpolation procedure using measurements at center-of-mass energies of 2.76 and 7 TeV [51]. The resulting backward-to-forward ratio of J/ψ production cross-section in pp collisions is 0.691 ± 0.048, leading to a global uncertainty on the $R_{\rm FB}$ measurement of 6.9%.

For the $R_{\rm FB}$ ratio, the systematic uncertainties of the absolute yields in p–Pb collisions (Tab. 3) are considered as uncorrelated between forward and backward rapidity, and therefore added in quadrature. The uncorrelated systematic uncertainties of the production cross sections in pp collisions are the same as a function of multiplicity, so they are added in quadrature to the global uncertainty. The muon trigger, tracking and matching efficiency uncertainties are uncorrelated over rapidity but correlated in multiplicity. They are therefore also added in quadrature to the global uncertainty resulting in a total relative uncertainty of 11%.

The $R_{\rm FB}$ ratio is shown as a function of the relative charged-particle pseudorapidity density in Fig. 5. In

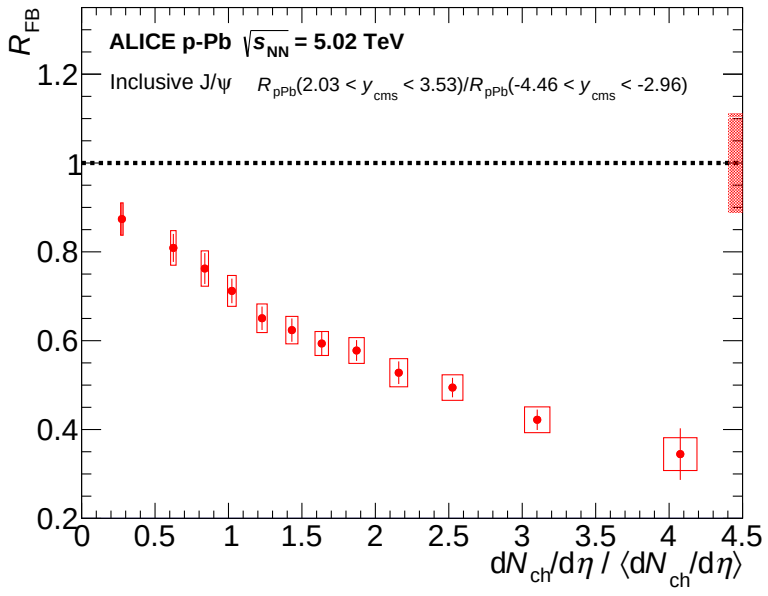

Fig. 5: $R_{\rm FB}$ of inclusive J/ψ in p-Pb collisions at $\sqrt{s_{\rm NN}} = 5.02$ TeV as a function of relative charged-particle pseudorapidity density. The red box around unity represents the global uncertainty. The error bars show the statistical uncertainties, the boxes the systematic ones.

inclusive collisions for symmetric y ranges [18], $R_{\rm FB}$ is smaller than unity and described by theoretical models. The present measurement shows that the suppression of J/ψ production at forward rapidity with respect to backward rapidity increases significantly with charged-particle multiplicity, since $R_{\rm FB}$ reaches values as low as 0.34 ± 0.06 (stat.) $\pm$ 0.05 (syst.). A forward-backward asymmetry can be noticed for inclusive charged-particle production studied in [50]. Even though the range of relative charged-particle multiplicities probed in that measurement is not as large as in the present measurement of J/ψ production, the apparent similarity of the trend seen in Fig. 5 to soft particle production is intriguing.

In Fig. 6 the relative $\langle p_{\rm T} \rangle$ of J/ψ mesons at backward and forward rapidity is shown as a function of the relative charged-particle pseudorapidity density. The results are similar at forward and backward rapidities. An increase of the relative $\langle p_{\rm T} \rangle$ with multiplicity at low charged-particle multiplicity is observed, but for multiplicities beyond 1.5 times the average multiplicity it saturates. For backward rapidity, the simultaneous increase of the yield and the saturation of the relative $\langle p_{\rm T} \rangle$ could be an indication of J/ψ production from an incoherent superposition of parton-parton interactions, as suggested by data on correlations of jet-like yields per trigger particle [32].

The $p_{\rm T}$ broadening observed in the analysis of J/ψ production in p–Pb collisions as a function of centrality [34] is well described by initial and final-state multiple scattering of partons within the nuclear medium [53]. The comparison of data to model calculations, performed in [34], corresponds in terms of relative multiplicities to a range up to roughly $\mathrm{d}N_{\rm ch}/\mathrm{d}\eta / \langle \mathrm{d}N_{\rm ch}/\mathrm{d}\eta \rangle = 2.5$. It remains to be seen whether such models can explain the saturation observed in the relative $\langle p_{\rm T} \rangle$ of the J/ψ mesons for events with higher multiplicities.

It is interesting to contrast the observed saturation of $\langle p_{\rm T} \rangle$ for J/ψ mesons with the monotonic increase of $\langle p_{\rm T} \rangle$ for charged hadrons (dominated by pion production) [54] with the multiplicity measured at mid-rapidity also shown in Fig. 6. Note that this measurement is for particles in $|\eta_{\rm cms}| < 0.3$ and with $p_{\rm T}$ in the range 0.15 to 10 GeV/c, and it is relative to events with at least one particle in this kinematic range (for which $\langle N_{\rm ch} \rangle = 11.9 \pm 0.5$ and $\langle p_{\rm T} \rangle = 0.696 \pm 0.024$ GeV/c [54]). Although the different kinematic regions may play a role and care is needed in the interpretation, it is apparent that the two

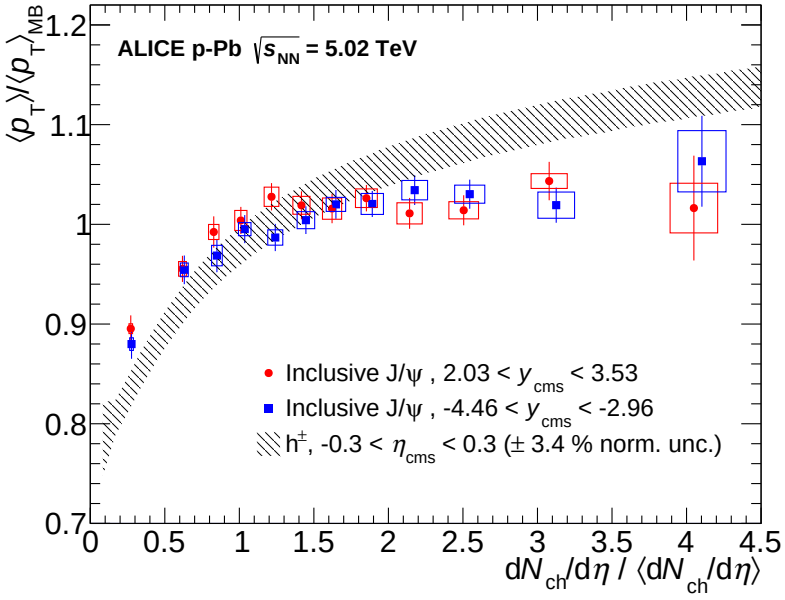
ALICE p-Pb $\sqrt{s_{NN}}$ = 5.02 TeV
Inclusive J/ψ , 2.03 < y_{cms} < 3.53
Inclusive J/ψ , -4.46 < y_{cms} < -2.96
h±, -0.3 < η_{cms} < 0.3 (± 3.4 % norm. unc.)
$\langle p_T \rangle / \langle p_T \rangle_{MB}$
$dN_{ch}/d\eta$ / $\langle dN_{ch}/d\eta \rangle$

Fig. 6: Relative $\langle p_{\mathrm{T}} \rangle$ of J/ψ mesons for backward and forward rapidity as a function of the relative charged-particle pseudorapidity density. The bars show the statistical uncertainties, the boxes the systematic ones. The data for charged particles ($\mathrm{h}^{\pm}$) [52] are included for comparison. The latter are for $|\eta_{\mathrm{cms}}| < 0.3$ and with p_{T} in the range 0.15 to 10 GeV/c and have an additional normalisation uncertainty of 3.4%.

observables, characterised by rather different production mechanisms (and momentum-transfer) exhibit different patterns in the multiplicity dependence of the average transverse momenta.

7 Conclusions

Measurements of the relative J/ψ yield and average transverse momentum as a function of the relative charged-particle pseudorapidity density in p–Pb collisions at the LHC at $\sqrt{s_{\mathrm{NN}}} = 5.02$ TeV have been presented in this letter. The measurements were performed with ALICE in three ranges of rapidity. The charged-particle multiplicity was measured at mid-rapidity; multiplicities up to 4 times the value of NSD events were reached, corresponding to rare events of less than 1% of the total hadronic interaction cross section. An increase of the relative J/ψ yield with the relative multiplicity was observed, with a trend towards saturation at high multiplicity for the forward rapidity (proton-going direction). For the J/ψ data at mid-rapidity, a comparison to corresponding measurements of D-meson yields was performed, revealing similar patterns for the two meson species. At forward and backward rapidities, the relative average transverse momentum exhibits a saturation above moderate values of relative multiplicity.

The present data are expected to constitute a stringent test for theoretical models of J/ψ production in p–Pb collisions and they will help to understand the connection to effects associated with the production of a deconfined medium in Pb–Pb collisions. The measurements reported here may help to clarify whether such a medium is also produced in high-multiplicity p–Pb collisions.

Acknowledgements

The ALICE Collaboration would like to thank all its engineers and technicians for their invaluable contributions to the construction of the experiment and the CERN accelerator teams for the outstanding performance of the LHC complex. The ALICE Collaboration gratefully acknowledges the resources and support provided by all Grid centres and the Worldwide LHC Computing Grid (WLCG) collaboration.

The ALICE Collaboration acknowledges the following funding agencies for their support in building and running the ALICE detector: A. I. Alikhanyan National Science Laboratory (Yerevan Physics Institute) Foundation (ANSL), State Committee of Science and World Federation of Scientists (WFS), Armenia; Austrian Academy of Sciences and Nationalstiftung für Forschung, Technologie und Entwicklung, Austria; Ministry of Communications and High Technologies, National Nuclear Research Center, Azerbaijan; Conselho Nacional de Desenvolvimento Científico e Tecnológico (CNPq), Universidade Federal do Rio Grande do Sul (UFRGS), Financiadora de Estudos e Projetos (Finep) and Fundação de Amparo à Pesquisa do Estado de São Paulo (FAPESP), Brazil; Ministry of Science & Technology of China (MSTC), National Natural Science Foundation of China (NSFC) and Ministry of Education of China (MOEC) , China; Ministry of Science, Education and Sport and Croatian Science Foundation, Croatia; Ministry of Education, Youth and Sports of the Czech Republic, Czech Republic; The Danish Council for Independent Research — Natural Sciences, the Carlsberg Foundation and Danish National Research Foundation (DNRF), Denmark; Helsinki Institute of Physics (HIP), Finland; Commissariat à l'Energie Atomique (CEA) and Institut National de Physique Nucléaire et de Physique des Particules (IN2P3) and Centre National de la Recherche Scientifique (CNRS), France; Bundesministerium für Bildung, Wissenschaft, Forschung und Technologie (BMBF) and GSI Helmholtzzentrum für Schwerionenforschung GmbH, Germany; Ministry of Education, Research and Religious Affairs, Greece; National Research, Development and Innovation Office, Hungary; Department of Atomic Energy Government of India (DAE) and Council of Scientific and Industrial Research (CSIR), New Delhi, India; Indonesian Institute of Science, Indonesia; Centro Fermi - Museo Storico della Fisica e Centro Studi e Ricerche Enrico Fermi and Istituto Nazionale di Fisica Nucleare (INFN), Italy; Institute for Innovative Science and Technology , Nagasaki Institute of Applied Science (IIST), Japan Society for the Promotion of Science (JSPS) KAKENHI and Japanese Ministry of Education, Culture, Sports, Science and Technology (MEXT), Japan; Consejo Nacional de Ciencia (CONACYT) y Tecnología, through Fondo de Cooperación Internacional en Ciencia y Tecnología (FONCICYT) and Dirección General de Asuntos del Personal Academico (DGAPA), Mexico; Nederlandse Organisatie voor Wetenschappelijk Onderzoek (NWO), Netherlands; The Research Council of Norway, Norway; Commission on Science and Technology for Sustainable Development in the South (COMSATS), Pakistan; Pontificia Universidad Católica del Perú, Peru; Ministry of Science and Higher Education and National Science Centre, Poland; Korea Institute of Science and Technology Information and National Research Foundation of Korea (NRF), Republic of Korea; Ministry of Education and Scientific Research, Institute of Atomic Physics and Romanian National Agency for Science, Technology and Innovation, Romania; Joint Institute for Nuclear Research (JINR), Ministry of Education and Science of the Russian Federation and National Research Centre Kurchatov Institute, Russia; Ministry of Education, Science, Research and Sport of the Slovak Republic, Slovakia; National Research Foundation of South Africa, South Africa; Centro de Aplicaciones Tecnológicas y Desarrollo Nuclear (CEADEN), Cubaenergía, Cuba, Ministerio de Ciencia e Innovacion and Centro de Investigaciones Energéticas, Medioambientales y Tecnológicas (CIEMAT), Spain; Swedish Research Council (VR) and Knut & Alice Wallenberg Foundation (KAW), Sweden; European Organization for Nuclear Research, Switzerland; National Science and Technology Development Agency (NSDTA), Suranaree University of Technology (SUT) and Office of the Higher Education Commission under NRU project of Thailand, Thailand; Turkish Atomic Energy Agency (TAEK), Turkey; National Academy of Sciences of Ukraine, Ukraine; Science and Technology Facilities Council (STFC), United Kingdom; National Science Foundation of the United States of America (NSF) and United States Department of Energy, Office of Nuclear Physics (DOE NP), United States of America.

References

[1] T. Matsui and H. Satz, "J/ψ suppression by quark-gluon plasma formation," *Phys. Lett.* **B178** (1986) 416–422.

[2] **NA50** Collaboration, B. Alessandro *et al.*, "A new measurement of J/ψ suppression in Pb-Pb collisions at 158 GeV per nucleon," *Eur. Phys. J.* **C39** (2005) 335–345, arXiv:0412036.

[3] **NA60** Collaboration, R. Arnaldi *et al.*, "J/ψ production in Indium-Indium collisions at 158 GeV/Nucleon," *Phys. Rev. Lett.* **99** (2007) 132302.

[4] **PHENIX** Collaboration, A. Adare *et al.*, "J/ψ suppression at forward rapidity in Au+Au collisions at $\sqrt{s_{\rm NN}} = 200$ GeV," *Phys. Rev.* **C84** (2011) 054912, arXiv:1103.6269.

[5] **ALICE** Collaboration, B. Abelev *et al.*, "J/ψ suppression at forward rapidity in Pb-Pb collisions at $\sqrt{s_{\rm NN}} = 2.76$ TeV," *Phys. Rev. Lett.* **109** (2012) 072301, arXiv:1202.1383.

[6] **STAR** Collaboration, L. Adamczyk *et al.*, "J/ψ production at low p_T in Au+Au and Cu+Cu collisions at $\sqrt{s_{NN}} = 200$ GeV with the STAR detector," *Phys. Rev.* **C90** (2014) 024906, arXiv:1310.3563.

[7] **ALICE** Collaboration, B. Abelev *et al.*, "Centrality, rapidity and transverse momentum dependence of J/ψ suppression in Pb-Pb collisions at $\sqrt{s_{\rm NN}}$=2.76 TeV," *Phys. Lett.* **B734** (2014) 314–327, arXiv:1311.0214.

[8] **CMS** Collaboration, S. Chatrchyan *et al.*, "Suppression of non-prompt J/ψ, prompt J/ψ, and Υ(1S) in Pb-Pb collisions at $\sqrt{s_{\rm NN}}$ =2.76 TeV," *JHEP* **1205** (2012) 063, arXiv:1201.5069.

[9] **ATLAS** Collaboration, G. Aad *et al.*, "Measurement of the centrality dependence of J/ψ yields and observation of Z production in lead-lead collisions with the ATLAS detector at the LHC," *Phys. Lett.* **B697** (2011) 294–312, arXiv:1012.5419.

[10] **ALICE** Collaboration, J. Adam *et al.*, "J/ψ suppression at forward rapidity in Pb-Pb collisions at $\sqrt{\mathbf{s}_{\rm NN}} = \mathbf{5.02}$ TeV," *Phys. Lett.* **B766** (2017) 212–224, arXiv:1606.08197.

[11] C. Salgado *et al.*, "Proton-Nucleus Collisions at the LHC: Scientific Opportunities and Requirements," *J. Phys.* **G39** (2012) 015010, arXiv:1105.3919.

[12] R. Vogt *et al.*, "Predictions for p+Pb collisions at $\sqrt{s_{\rm NN}} = 5$ TeV," *Int.J.Mod.Phys.* **E22** (2013) 1330007, arXiv:1301.3395.

[13] F. Arleo and S. Peigné, "Heavy-quarkonium suppression in p-A collisions from parton energy loss in cold QCD matter," *JHEP* **1303** (2013) 122, arXiv:1212.0434.

[14] **PHENIX** Collaboration, A. Adare *et al.*, "Cold nuclear matter effects on J/ψ as constrained by deuteron-gold measurements at $\sqrt{s_{\rm NN}} = 200$ GeV," *Phys. Rev.* **C77** (2008) 024912, arXiv:1305.5516.

[15] **PHENIX** Collaboration, A. Adare *et al.*, "Cold nuclear matter effects on J/ψ yields as a function of rapidity and nuclear geometry in d+Au collisions at $\sqrt{s_{\rm NN}}$ =200 GeV," *Phys. Rev. Lett.* **107** (2011) 142301, arXiv:1010.1246.

[16] **PHENIX** Collaboration, A. Adare *et al.*, "Transverse-momentum dependence of the J/ψ nuclear modification in d+Au collisions at $\sqrt{s_{\rm NN}} = 200$ GeV," *Phys. Rev.* **C87** (2013) 034904, arXiv:1204.0777.

[17] **LHCb** Collaboration, R. Aaij *et al.*, "Study of J/ψ production and cold nuclear matter effects in p-Pb collisions at $\sqrt{s_{NN}} = 5$ TeV," *JHEP* **02** (2014) 072, arXiv:1308.6729.

[18] **ALICE** Collaboration, B. Abelev *et al.*, "J/ψ production and nuclear effects in p-Pb collisions at $\sqrt{s_{\rm NN}}$ = 5.02 TeV," *JHEP* **1402** (2014) 073, arXiv:1308.6726.

[19] **ALICE** Collaboration, J. Adam *et al.*, "Rapidity and transverse-momentum dependence of the inclusive J/ψ nuclear modification factor in p-Pb collisions at $\sqrt{s_{\rm NN}} = 5.02$ TeV," *JHEP* **06** (2015) 055, arXiv:1503.07179.

[20] Y.-Q. Ma, R. Venugopalan, and H.-F. Zhang, "J/ψ production and suppression in high energy proton-nucleus collisions," *Phys. Rev.* **D92** (2015) 071901, arXiv:1503.07772.

[21] B. Ducloué, T. Lappi, and H. Mäntysaari, "Forward J/ψ production in proton-nucleus collisions at high energy," *Phys. Rev.* **D91** no. 11, (2015) 114005, arXiv:1503.02789.

[22] **LHCb** Collaboration, R. Aaij *et al.*, "Study of Υ production and cold nuclear matter effects in p-Pb collisions at $\sqrt{s_{\rm NN}} = 5$ TeV," *JHEP* **1407** (2014) 094, arXiv:1405.5152.

[23] **ALICE** Collaboration, B. Abelev *et al.*, "Production of inclusive Υ(1S) and Υ(2S) in p-Pb collisions at 5.02 TeV," *Phys. Lett.* **B740** (2015) 105–117, arXiv:1410.2234.

[24] **ALICE** Collaboration, B. Abelev *et al.*, "Suppression of ψ(2S) production in p-Pb collisions at $\sqrt{s_{\rm NN}} = 5.02$ TeV," *JHEP* **1412** (2014) 073, arXiv:1405.3796.

[25] **LHCb** Collaboration, R. Aaij *et al.*, "Study of $\psi(2S)$ production and cold nuclear matter effects in pPb collisions at $\sqrt{s_{NN}} = 5$ TeV," *JHEP* **1603** (2016) 133, arXiv:1601.07878.

[26] **CMS** Collaboration, S. Chatrchyan *et al.*, "Observation of long-range near-side angular correlations in proton-lead collisions at the LHC," *Phys. Lett.* **B718** (2013) 795–814, arXiv:1210.5482.

[27] **ALICE** Collaboration, B. Abelev *et al.*, "Long-range angular correlations on the near and away side in p-Pb collisions at $\sqrt{s_{\rm NN}} = 5.02$ TeV," *Phys. Lett.* **B719** (2013) 29–41, arXiv:1212.2001.

[28] **ATLAS** Collaboration, G. Aad *et al.*, "Measurement with the ATLAS detector of multi-particle azimuthal correlations in p+Pb collisions at $\sqrt{s_{\rm NN}} = 5.02$ TeV," *Phys. Lett.* **B725** (2013) 60–78, arXiv:1303.2084.

[29] **ALICE** Collaboration, B. Abelev *et al.*, "Long-range angular correlations of π, k and p in p-Pb collisions at $\sqrt{s_{\rm NN}} = 5.02$ TeV," *Phys. Lett.* **B726** (2013) 164–177, arXiv:1307.3237.

[30] **CMS** Collaboration, S. Chatrchyan *et al.*, "Multiplicity and transverse momentum dependence of two-and four-particle correlations in p-Pb and Pb-Pb collisions," *Phys. Lett.* **B724** (2013) 213–240, arXiv:1305.0609.

[31] **ALICE** Collaboration, B. Abelev *et al.*, "Multiparticle azimuthal correlations in p-Pb and Pb-Pb collisions at the CERN Large Hadron Collider," *Phys. Rev.* **C90** (2014) 054901, arXiv:1406.2474.

[32] **ALICE** Collaboration, B. Abelev *et al.*, "Multiplicity dependence of jet-like two-particle correlations in p-Pb collisions at $\sqrt{s_{\rm NN}} = 5.02$ TeV," *Phys. Lett.* **B741** (2015) 38–50, arXiv:1406.5463.

[33] **ALICE** Collaboration, B. Abelev *et al.*, "Multiplicity Dependence of Pion, Kaon, Proton and Lambda Production in p-Pb Collisions at $\sqrt{s_{NN}} = 5.02$ TeV," *Phys. Lett.* **B728** (2014) 25–38, arXiv:1307.6796.

[34] **ALICE** Collaboration, J. Adam *et al.*, "Centrality dependence of inclusive J/ψ production in p-Pb collisions at $\sqrt{s_{\rm NN}} = 5.02$ TeV," *JHEP* **11** (2015) 127, arXiv:1506.08808.

[35] **CMS** Collaboration, S. Chatrchyan *et al.*, "Event activity dependence of $\Upsilon(nS)$ production in $\sqrt{s_{\rm NN}}$ = 5.02 TeV p-Pb and $\sqrt{s}$ = 2.76 TeV pp collisions," *JHEP* **1404** (2014) 103, arXiv:1312.6300.

[36] **ALICE** Collaboration, J. Adam *et al.*, "Measurement of D-meson production versus multiplicity in p-Pb collisions at $\sqrt{s_{\rm NN}} = 5.02$ TeV," *JHEP* **1608** (2016) 078, arXiv:1602.07240.

[37] **ALICE** Collaboration, B. Abelev *et al.*, "J/ψ production as a function of charged particle multiplicity in pp collisions at $\sqrt{s} = 7$ TeV," *Phys. Lett.* **B712** (2012) 165–175, arXiv:1202.2816.

[38] **ALICE** Collaboration, J. Adam *et al.*, "Measurement of charm and beauty production at central rapidity versus charged-particle multiplicity in proton-proton collisions at $\sqrt{s} = 7$ TeV," *JHEP* **09** (2015) 148, arXiv:1505.00664.

[39] **ALICE** Collaboration, J. Adam *et al.*, "Centrality dependence of ψ(2S) suppression in p-Pb collisions at $\sqrt{s_{\rm NN}}$ = 5.02 TeV," *JHEP* **06** (2016) 050, arXiv:1603.02816.

[40] **ALICE** Collaboration, B. Abelev *et al.*, "The ALICE experiment at the CERN LHC," *JINST* **3** (2008) S08002.

[41] **ALICE** Collaboration, B. Abelev *et al.*, "Performance of the ALICE Experiment at the CERN LHC," *Int. J. Mod. Phys.* **A29** (2014) 1430044, arXiv:1402.4476.

[42] **ALICE** Collaboration, B. Abelev *et al.*, "Pseudorapidity density of charged particles in p-Pb collisions at $\sqrt{s_{\rm NN}} = 5.02$ TeV," *Phys. Rev. Lett.* **110** (2013) 032301, arXiv:1210.3615.

[43] S. Roesler, R. Engel, and J. Ranft, "The Monte Carlo event generator DPMJET-III," arXiv:hep-ph/0012252.

[44] R. Brun *et al.*, "GEANT Detector Description and Simulation Tool," *CERN-W5013, CERN-W-5013, W5013, W-5013* (1994) .

[45] X.-N. Wang and M. Gyulassy, "HIJING: A Monte Carlo model for multiple jet production in pp, pA and AA collisions," *Phys. Rev.* **D44** (1991) 3501–3516.

[46] D. Lange, "The EvtGen particle decay simulation package," *Nucl. Instrum. Meth. A* **462** (2001) 152–155.

[47] E. Barberio, B. van Eijk, and Z. Was, "PHOTOS – a universal Monte Carlo for QED radiative corrections in decays," *Computer Physics Communications* **66** (1991) 115 – 128.

[48] E. Barberio and Z. Was, "PHOTOS – a universal Monte Carlo for QED radiative corrections: version 2.0," *Computer Physics Communications* **79** (1994) 291 – 308.

[49] E. G. Ferreiro, "Excited charmonium suppression in proton–nucleus collisions as a consequence of comovers," *Phys. Lett.* **B749** (2015) 98–103, arXiv:1411.0549.

[50] **ALICE** Collaboration, J. Adam *et al.*, "Centrality dependence of particle production in p-Pb collisions at $\sqrt{s_{\rm NN}}$= 5.02 TeV," *Phys. Rev.* **C91** (2015) 064905, arXiv:1412.6828.

[51] **LHCb, ALICE** Collaboration, "Reference pp cross-sections for J/ψ studies in proton-lead collisions at $\sqrt{s_{NN}} = 5.02$ TeV and comparisons between ALICE and LHCb results," *LHCb-CONF-2013-013, CERN-LHCb-CONF-2013-013, ALICE-PUBLIC-2013-002"* (2013) .

[52] **ALICE** Collaboration, B. Abelev *et al.*, "Multiplicity dependence of the average transverse momentum in pp, p-Pb and Pb-Pb collisions at the LHC," *Phys. Lett.* **B727** (2013) 371–380, arXiv:1307.1094.

[53] Z.-B. Kang and J.-W. Qiu, "Nuclear modification of vector boson production in proton-lead collisions at the LHC," *Phys. Lett.* **B721** (2013) 277–283, arXiv:1212.6541.

[54] **ALICE** Collaboration, B. Abelev *et al.*, "Multiplicity dependence of the average transverse momentum in pp, p-Pb, and Pb-Pb collisions at the LHC," *Phys. Lett.* **B727** (2013) 371–380, arXiv:1307.1094.

A The ALICE Collaboration

D. Adamová[87], M.M. Aggarwal[91], G. Aglieri Rinella[34], M. Agnello[30], N. Agrawal[47], Z. Ahammed[139], N. Ahmad[17], S.U. Ahn[69], S. Aiola[143], A. Akindinov[54], S.N. Alam[139], D.S.D. Albuquerque[124], D. Aleksandrov[83], B. Alessandro[113], D. Alexandre[104], R. Alfaro Molina[64], A. Alici[26,12,107], A. Alkin[3], J. Alme[21], T. Alt[41], I. Altsybeev[138], C. Alves Garcia Prado[123], M. An[7], C. Andrei[80], H.A. Andrews[104], A. Andronic[100], V. Anguelov[96], C. Anson[90], T. Antičić[101], F. Antinori[110], P. Antonioli[107], R. Anwar[126], L. Aphecetche[116], H. Appelshäuser[60], S. Arcelli[26], R. Arnaldi[113], O.W. Arnold[97,35], I.C. Arsene[20], M. Arslandok[60], B. Audurier[116], A. Augustinus[34], R. Averbeck[100], M.D. Azmi[17], A. Badalà[109], Y.W. Baek[68], S. Bagnasco[113], R. Bailhache[60], R. Bala[93], A. Baldisseri[65], M. Ball[44], R.C. Baral[57], A.M. Barbano[25], R. Barbera[27], F. Barile[32,106], L. Barioglio[25], G.G. Barnaföldi[142], L.S. Barnby[34,104], V. Barret[71], P. Bartalini[7], K. Barth[34], J. Bartke[120,i], E. Bartsch[60], M. Basile[26], N. Bastid[71], S. Basu[139], B. Bathen[61], G. Batigne[116], A. Batista Camejo[71], B. Batyunya[67], P.C. Batzing[20], I.G. Bearden[84], H. Beck[96], C. Bedda[30], N.K. Behera[50], I. Belikov[135], F. Bellini[26], H. Bello Martinez[2], R. Bellwied[126], L.G.E. Beltran[122], V. Belyaev[76], G. Bencedi[142], S. Beole[25], A. Bercuci[80], Y. Berdnikov[89], D. Berenyi[142], R.A. Bertens[53,129], D. Berzano[34], L. Betev[34], A. Bhasin[93], I.R. Bhat[93], A.K. Bhati[91], B. Bhattacharjee[43], J. Bhom[120], L. Bianchi[126], N. Bianchi[73], C. Bianchin[141], J. Bielčík[38], J. Bielčíková[87], A. Bilandzic[35,97], G. Biro[142], R. Biswas[4], S. Biswas[4], J.T. Blair[121], D. Blau[83], C. Blume[60], G. Boca[136], F. Bock[75,96], A. Bogdanov[76], L. Boldizsár[142], M. Bombara[39], G. Bonomi[137], M. Bonora[34], J. Book[60], H. Borel[65], A. Borissov[99], M. Borri[128], E. Botta[25], C. Bourjau[84], P. Braun-Munzinger[100], M. Bregant[123], T.A. Broker[60], T.A. Browning[98], M. Broz[38], E.J. Brucken[45], E. Bruna[113], G.E. Bruno[32], D. Budnikov[102], H. Buesching[60], S. Bufalino[30], P. Buhler[115], S.A.I. Buitron[62], P. Buncic[34], O. Busch[132], Z. Buthelezi[66], J.B. Butt[15], J.T. Buxton[18], J. Cabala[118], D. Caffarri[34], H. Caines[143], A. Caliva[53], E. Calvo Villar[105], P. Camerini[24], A.A. Capon[115], F. Carena[34], W. Carena[34], F. Carnesecchi[12,26], J. Castillo Castellanos[65], A.J. Castro[129], E.A.R. Casula[23,108], C. Ceballos Sanchez[9], P. Cerello[113], B. Chang[127], S. Chapeland[34], M. Chartier[128], J.L. Charvet[65], S. Chattopadhyay[139], S. Chattopadhyay[103], A. Chauvin[97,35], M. Cherney[90], C. Cheshkov[134], B. Cheynis[134], V. Chibante Barroso[34], D.D. Chinellato[124], S. Cho[50], P. Chochula[34], K. Choi[99], M. Chojnacki[84], S. Choudhury[139], P. Christakoglou[85], C.H. Christensen[84], P. Christiansen[33], T. Chujo[132], S.U. Chung[99], C. Cicalo[108], L. Cifarelli[12,26], F. Cindolo[107], J. Cleymans[92], F. Colamaria[32], D. Colella[55,34], A. Collu[75], M. Colocci[26], G. Conesa Balbastre[72], Z. Conesa del Valle[51], M.E. Connors[143,ii], J.G. Contreras[38], T.M. Cormier[88], Y. Corrales Morales[113], I. Cortés Maldonado[2], P. Cortese[31], M.R. Cosentino[125], F. Costa[34], S. Costanza[136], J. Crkovská[51], P. Crochet[71], E. Cuautle[62], L. Cunqueiro[61], T. Dahms[35,97], A. Dainese[110], M.C. Danisch[96], A. Danu[58], D. Das[103], I. Das[103], S. Das[4], A. Dash[81], S. Dash[47], S. De[48,123], A. De Caro[29], G. de Cataldo[106], C. de Conti[123], J. de Cuveland[41], A. De Falco[23], D. De Gruttola[12,29], N. De Marco[113], S. De Pasquale[29], R.D. De Souza[124], H.F. Degenhardt[123], A. Deisting[100,96], A. Deloff[79], C. Deplano[85], P. Dhankher[47], D. Di Bari[32], A. Di Mauro[34], P. Di Nezza[73], B. Di Ruzza[110], M.A. Diaz Corchero[10], T. Dietel[92], P. Dillenseger[60], R. Divià[34], Ø. Djuvsland[21], A. Dobrin[58,34], D. Domenicis Gimenez[123], B. Dönigus[60], O. Dordic[20], T. Drozhzhova[60], A.K. Dubey[139], A. Dubla[100], L. Ducroux[134], A.K. Duggal[91], P. Dupieux[71], R.J. Ehlers[143], D. Elia[106], E. Endress[105], H. Engel[59], E. Epple[143], B. Erazmus[116], F. Erhardt[133], B. Espagnon[51], S. Esumi[132], G. Eulisse[34], J. Eum[99], D. Evans[104], S. Evdokimov[114], L. Fabbietti[35,97], J. Faivre[72], A. Fantoni[73], M. Fasel[88,75], L. Feldkamp[61], A. Feliciello[113], G. Feofilov[138], J. Ferencei[87], A. Fernández Téllez[2], E.G. Ferreiro[16], A. Ferretti[25], A. Festanti[28], V.J.G. Feuillard[71,65], J. Figiel[120], M.A.S. Figueredo[123], S. Filchagin[102], D. Finogeev[52], F.M. Fionda[23], E.M. Fiore[32], M. Floris[34], S. Foertsch[66], P. Foka[100], S. Fokin[83], E. Fragiacomo[112], A. Francescon[34], A. Francisco[116], U. Frankenfeld[100], G.G. Fronze[25], U. Fuchs[34], C. Furget[72], A. Furs[52], M. Fusco Girard[29], J.J. Gaardhøje[84], M. Gagliardi[25], A.M. Gago[105], K. Gajdosova[84], M. Gallio[25], C.D. Galvan[122], P. Ganoti[78], C. Gao[7], C. Garabatos[100], E. Garcia-Solis[13], K. Garg[27], P. Garg[48], C. Gargiulo[34], P. Gasik[35,97], E.F. Gauger[121], M.B. Gay Ducati[63], M. Germain[116], P. Ghosh[139], S.K. Ghosh[4], P. Gianotti[73], P. Giubellino[34,113], P. Giubilato[28], E. Gladysz-Dziadus[120], P. Glässel[96], D.M. Goméz Coral[64], A. Gomez Ramirez[59], A.S. Gonzalez[34], V. Gonzalez[10], P. González-Zamora[10], S. Gorbunov[41], L. Görlich[120], S. Gotovac[119], V. Grabski[64], L.K. Graczykowski[140], K.L. Graham[104], L. Greiner[75], A. Grelli[53], C. Grigoras[34], V. Grigoriev[76], A. Grigoryan[1], S. Grigoryan[67], N. Grion[112], J.M. Gronefeld[100], F. Grosa[30], J.F. Grosse-Oetringhaus[34], R. Grosso[100], L. Gruber[115], F.R. Grull[59], F. Guber[52], R. Guernane[72], B. Guerzoni[26], K. Gulbrandsen[84], T. Gunji[131], A. Gupta[93], R. Gupta[93], I.B. Guzman[2], R. Haake[34], C. Hadjidakis[51], H. Hamagaki[77,131], G. Hamar[142], J.C. Hamon[135], J.W. Harris[143], A. Harton[13], D. Hatzifotiadou[107], S. Hayashi[131], S.T. Heckel[60], E. Hellbär[60], H. Helstrup[36], A. Herghelegiu[80], G. Herrera Corral[11], F. Herrmann[61], B.A. Hess[95], K.F. Hetland[36], H. Hillemanns[34], B. Hippolyte[135], J. Hladky[56], B. Hohlweger[97], D. Horak[38], R. Hosokawa[132], P. Hristov[34], C. Hughes[129], T.J. Humanic[18], N. Hussain[43], T. Hussain[17], D. Hutter[41], D.S. Hwang[19], R. Ilkaev[102],

M. Inaba[132], M. Ippolitov[83,76], M. Irfan[17], V. Isakov[52], M.S. Islam[48], M. Ivanov[34,100], V. Ivanov[89], V. Izucheev[114], B. Jacak[75], N. Jacazio[26], P.M. Jacobs[75], M.B. Jadhav[47], S. Jadlovska[118], J. Jadlovsky[118], S. Jaelani[53], C. Jahnke[35], M.J. Jakubowska[140], M.A. Janik[140], P.H.S.Y. Jayarathna[126], C. Jena[81], S. Jena[126], M. Jercic[133], R.T. Jimenez Bustamante[100], P.G. Jones[104], A. Jusko[104], P. Kalinak[55], A. Kalweit[34], J.H. Kang[144], V. Kaplin[76], S. Kar[139], A. Karasu Uysal[70], O. Karavichev[52], T. Karavicheva[52], L. Karayan[100,96], E. Karpechev[52], U. Kebschull[59], R. Keidel[145], D.L.D. Keijdener[53], M. Keil[34], B. Ketzer[44], M. Mohisin Khan[17,iii], P. Khan[103], S.A. Khan[139], A. Khanzadeev[89], Y. Kharlov[114], A. Khatun[17], A. Khuntia[48], M.M. Kielbowicz[120], B. Kileng[36], D.W. Kim[42], D.J. Kim[127], D. Kim[144], H. Kim[144], J.S. Kim[42], J. Kim[96], M. Kim[50], M. Kim[144], S. Kim[19], T. Kim[144], S. Kirsch[41], I. Kisel[41], S. Kiselev[54], A. Kisiel[140], G. Kiss[142], J.L. Klay[6], C. Klein[60], J. Klein[34], C. Klein-Bösing[61], S. Klewin[96], A. Kluge[34], M.L. Knichel[96], A.G. Knospe[126], C. Kobdaj[117], M. Kofarago[34], T. Kollegger[100], A. Kolojvari[138], V. Kondratiev[138], N. Kondratyeva[76], E. Kondratyuk[114], A. Konevskikh[52], M. Kopcik[118], M. Kour[93], C. Kouzinopoulos[34], O. Kovalenko[79], V. Kovalenko[138], M. Kowalski[120], G. Koyithatta Meethaleveedu[47], I. Králik[55], A. Kravčáková[39], M. Krivda[55,104], F. Krizek[87], E. Kryshen[89], M. Krzewicki[41], A.M. Kubera[18], V. Kučera[87], C. Kuhn[135], P.G. Kuijer[85], A. Kumar[93], J. Kumar[47], L. Kumar[91], S. Kumar[47], S. Kundu[81], P. Kurashvili[79], A. Kurepin[52], A.B. Kurepin[52], A. Kuryakin[102], S. Kushpil[87], M.J. Kweon[50], Y. Kwon[144], S.L. La Pointe[41], P. La Rocca[27], C. Lagana Fernandes[123], I. Lakomov[34], R. Langoy[40], K. Lapidus[143], C. Lara[59], A. Lardeux[20,65], A. Lattuca[25], E. Laudi[34], R. Lavicka[38], L. Lazaridis[34], R. Lea[24], L. Leardini[96], S. Lee[144], F. Lehas[85], S. Lehner[115], J. Lehrbach[41], R.C. Lemmon[86], V. Lenti[106], E. Leogrande[53], I. León Monzón[122], P. Lévai[142], S. Li[7], X. Li[14], J. Lien[40], R. Lietava[104], S. Lindal[20], V. Lindenstruth[41], C. Lippmann[100], M.A. Lisa[18], V. Litichevskyi[45], H.M. Ljunggren[33], W.J. Llope[141], D.F. Lodato[53], P.I. Loenne[21], V. Loginov[76], C. Loizides[75], P. Loncar[119], X. Lopez[71], E. López Torres[9], A. Lowe[142], P. Luettig[60], M. Lunardon[28], G. Luparello[24], M. Lupi[34], T.H. Lutz[143], A. Maevskaya[52], M. Mager[34], S. Mahajan[93], S.M. Mahmood[20], A. Maire[135], R.D. Majka[143], M. Malaev[89], I. Maldonado Cervantes[62], L. Malinina[67,iv], D. Mal'Kevich[54], P. Malzacher[100], A. Mamonov[102], V. Manko[83], F. Manso[71], V. Manzari[106], Y. Mao[7], M. Marchisone[130,66], J. Mareš[56], G.V. Margagliotti[24], A. Margotti[107], J. Margutti[53], A. Marín[100], C. Markert[121], M. Marquard[60], N.A. Martin[100], J. Martin Blanco[116], P. Martinengo[34], J.A.L. Martinez[59], M.I. Martínez[2], G. Martínez García[116], M. Martinez Pedreira[34], A. Mas[123], S. Masciocchi[100], M. Masera[25], A. Masoni[108], A. Mastroserio[32], A.M. Mathis[97,35], A. Matyja[120,129], C. Mayer[120], J. Mazer[129], M. Mazzilli[32], M.A. Mazzoni[111], F. Meddi[22], Y. Melikyan[76], A. Menchaca-Rocha[64], E. Meninno[29], J. Mercado Pérez[96], M. Meres[37], S. Mhlanga[92], Y. Miake[132], M.M. Mieskolainen[45], D.L. Mihaylov[97], K. Mikhaylov[54,67], L. Milano[75], J. Milosevic[20], A. Mischke[53], A.N. Mishra[48], D. Miśkowiec[100], J. Mitra[139], C.M. Mitu[58], N. Mohammadi[53], B. Mohanty[81], E. Montes[10], D.A. Moreira De Godoy[61], L.A.P. Moreno[2], S. Moretto[28], A. Morreale[116], A. Morsch[34], V. Muccifora[73], E. Mudnic[119], D. Mühlheim[61], S. Muhuri[139], M. Mukherjee[139,4], J.D. Mulligan[143], M.G. Munhoz[123], K. Münning[44], R.H. Munzer[60], H. Murakami[131], S. Murray[66], L. Musa[34], J. Musinsky[55], C.J. Myers[126], B. Naik[47], R. Nair[79], B.K. Nandi[47], R. Nania[107], E. Nappi[106], M.U. Naru[15], H. Natal da Luz[123], C. Nattrass[129], S.R. Navarro[2], K. Nayak[81], R. Nayak[47], T.K. Nayak[139], S. Nazarenko[102], A. Nedosekin[54], R.A. Negrao De Oliveira[34], L. Nellen[62], S.V. Nesbo[36], F. Ng[126], M. Nicassio[100], M. Niculescu[58], J. Niedziela[34], B.S. Nielsen[84], S. Nikolaev[83], S. Nikulin[83], V. Nikulin[89], F. Noferini[107,12], P. Nomokonov[67], G. Nooren[53], J.C.C. Noris[2], J. Norman[128], A. Nyanin[83], J. Nystrand[21], H. Oeschler[96,i], S. Oh[143], A. Ohlson[96,34], T. Okubo[46], L. Olah[142], J. Oleniacz[140], A.C. Oliveira Da Silva[123], M.H. Oliver[143], J. Onderwaater[100], C. Oppedisano[113], R. Orava[45], M. Oravec[118], A. Ortiz Velasquez[62], A. Oskarsson[33], J. Otwinowski[120], K. Oyama[77], Y. Pachmayer[96], V. Pacik[84], D. Pagano[137], P. Pagano[29], G. Paić[62], P. Palni[7], J. Pan[141], A.K. Pandey[47], S. Panebianco[65], V. Papikyan[1], G.S. Pappalardo[109], P. Pareek[48], J. Park[50], W.J. Park[100], S. Parmar[91], A. Passfeld[61], S.P. Pathak[126], V. Paticchio[106], R.N. Patra[139], B. Paul[113], H. Pei[7], T. Peitzmann[53], X. Peng[7], L.G. Pereira[63], H. Pereira Da Costa[65], D. Peresunko[83,76], E. Perez Lezama[60], V. Peskov[60], Y. Pestov[5], V. Petráček[38], V. Petrov[114], M. Petrovici[80], C. Petta[27], R.P. Pezzi[63], S. Piano[112], M. Pikna[37], P. Pillot[116], L.O.D.L. Pimentel[84], O. Pinazza[107,34], L. Pinsky[126], D.B. Piyarathna[126], M. Płoskoń[75], M. Planinic[133], J. Pluta[140], S. Pochybova[142], P.L.M. Podesta-Lerma[122], M.G. Poghosyan[88], B. Polichtchouk[114], N. Poljak[133], W. Poonsawat[117], A. Pop[80], H. Poppenborg[61], S. Porteboeuf-Houssais[71], J. Porter[75], J. Pospisil[87], V. Pozdniakov[67], S.K. Prasad[4], R. Preghenella[107,34], F. Prino[113], C.A. Pruneau[141], I. Pshenichnov[52], M. Puccio[25], G. Puddu[23], P. Pujahari[141], V. Punin[102], J. Putschke[141], H. Qvigstad[20], A. Rachevski[112], S. Raha[4], S. Rajput[93], J. Rak[127], A. Rakotozafindrabe[65], L. Ramello[31], F. Rami[135], D.B. Rana[126], R. Raniwala[94], S. Raniwala[94], S.S. Räsänen[45], B.T. Rascanu[60], D. Rathee[91], V. Ratza[44], I. Ravasenga[30], K.F. Read[88,129], K. Redlich[79], A. Rehman[21], P. Reichelt[60], F. Reidt[34], X. Ren[7], R. Renfordt[60], A.R. Reolon[73], A. Reshetin[52], K. Reygers[96], V. Riabov[89], R.A. Ricci[74], T. Richert[53,33], M. Richter[20], P. Riedler[34], W. Riegler[34], F. Riggi[27], C. Ristea[58], M. Rodríguez

Cahuantzi[2], K. Røed[20], E. Rogochaya[67], D. Rohr[41], D. Röhrich[21], P.S. Rokita[140], F. Ronchetti[34,73], L. Ronflette[116], P. Rosnet[71], A. Rossi[28], A. Rotondi[136], F. Roukoutakis[78], A. Roy[48], C. Roy[135], P. Roy[103], A.J. Rubio Montero[10], R. Rui[24], R. Russo[25], A. Rustamov[82], E. Ryabinkin[83], Y. Ryabov[89], A. Rybicki[120], S. Saarinen[45], S. Sadhu[139], S. Sadovsky[114], K. Šafařík[34], S.K. Saha[139], B. Sahlmuller[60], B. Sahoo[47], P. Sahoo[48], R. Sahoo[48], S. Sahoo[57], P.K. Sahu[57], J. Saini[139], S. Sakai[73,132], M.A. Saleh[141], J. Salzwedel[18], S. Sambyal[93], V. Samsonov[76,89], A. Sandoval[64], D. Sarkar[139], N. Sarkar[139], P. Sarma[43], M.H.P. Sas[53], E. Scapparone[107], F. Scarlassara[28], R.P. Scharenberg[98], H.S. Scheid[60], C. Schiaua[80], R. Schicker[96], C. Schmidt[100], H.R. Schmidt[95], M.O. Schmidt[96], M. Schmidt[95], S. Schuchmann[60], J. Schukraft[34], Y. Schutz[116,135,34], K. Schwarz[100], K. Schweda[100], G. Scioli[26], E. Scomparin[113], R. Scott[129], M. Šefčík[39], J.E. Seger[90], Y. Sekiguchi[131], D. Sekihata[46], I. Selyuzhenkov[76,100], K. Senosi[66], S. Senyukov[3,135,34], E. Serradilla[64,10], P. Sett[47], A. Sevcenco[58], A. Shabanov[52], A. Shabetai[116], O. Shadura[3], R. Shahoyan[34], A. Shangaraev[114], A. Sharma[93], A. Sharma[91], M. Sharma[93], M. Sharma[93], N. Sharma[129,91], A.I. Sheikh[139], K. Shigaki[46], Q. Shou[7], K. Shtejer[25,9], Y. Sibiriak[83], S. Siddhanta[108], K.M. Sielewicz[34], T. Siemiarczuk[79], D. Silvermyr[33], C. Silvestre[72], G. Simatovic[133], G. Simonetti[34], R. Singaraju[139], R. Singh[81], V. Singhal[139], T. Sinha[103], B. Sitar[37], M. Sitta[31], T.B. Skaali[20], M. Slupecki[127], N. Smirnov[143], R.J.M. Snellings[53], T.W. Snellman[127], J. Song[99], M. Song[144], F. Soramel[28], S. Sorensen[129], F. Sozzi[100], E. Spiriti[73], I. Sputowska[120], B.K. Srivastava[98], J. Stachel[96], I. Stan[58], P. Stankus[88], E. Stenlund[33], J.H. Stiller[96], D. Stocco[116], P. Strmen[37], A.A.P. Suaide[123], T. Sugitate[46], C. Suire[51], M. Suleymanov[15], M. Suljic[24], R. Sultanov[54], M. Šumbera[87], S. Sumowidagdo[49], K. Suzuki[115], S. Swain[57], A. Szabo[37], I. Szarka[37], A. Szczepankiewicz[140], M. Szymanski[140], U. Tabassam[15], J. Takahashi[124], G.J. Tambave[21], N. Tanaka[132], M. Tarhini[51], M. Tariq[17], M.G. Tarzila[80], A. Tauro[34], G. Tejeda Muñoz[2], A. Telesca[34], K. Terasaki[131], C. Terrevoli[28], B. Teyssier[134], D. Thakur[48], S. Thakur[139], D. Thomas[121], R. Tieulent[134], A. Tikhonov[52], A.R. Timmins[126], A. Toia[60], S. Tripathy[48], S. Trogolo[25], G. Trombetta[32], V. Trubnikov[3], W.H. Trzaska[127], B.A. Trzeciak[53], T. Tsuji[131], A. Tumkin[102], R. Turrisi[110], T.S. Tveter[20], K. Ullaland[21], E.N. Umaka[126], A. Uras[134], G.L. Usai[23], A. Utrobicic[133], M. Vala[118,55], J. Van Der Maarel[53], J.W. Van Hoorne[34], M. van Leeuwen[53], T. Vanat[87], P. Vande Vyvre[34], D. Varga[142], A. Vargas[2], M. Vargyas[127], R. Varma[47], M. Vasileiou[78], A. Vasiliev[83], A. Vauthier[72], O. Vázquez Doce[97,35], V. Vechernin[138], A.M. Veen[53], A. Velure[21], E. Vercellin[25], S. Vergara Limón[2], R. Vernet[8], R. Vértesi[142], L. Vickovic[119], S. Vigolo[53], J. Viinikainen[127], Z. Vilakazi[130], O. Villalobos Baillie[104], A. Villatoro Tello[2], A. Vinogradov[83], L. Vinogradov[138], T. Virgili[29], V. Vislavicius[33], A. Vodopyanov[67], M.A. Völkl[96], K. Voloshin[54], S.A. Voloshin[141], G. Volpe[32], B. von Haller[34], I. Vorobyev[97,35], D. Voscek[118], D. Vranic[34,100], J. Vrláková[39], B. Wagner[21], J. Wagner[100], H. Wang[53], M. Wang[7], D. Watanabe[132], Y. Watanabe[131], M. Weber[115], S.G. Weber[100], D.F. Weiser[96], J.P. Wessels[61], U. Westerhoff[61], A.M. Whitehead[92], J. Wiechula[60], J. Wikne[20], G. Wilk[79], J. Wilkinson[96], G.A. Willems[61], M.C.S. Williams[107], B. Windelband[96], M. Winn[96], W.E. Witt[129], S. Yalcin[70], P. Yang[7], S. Yano[46], Z. Yin[7], H. Yokoyama[132,72], I.-K. Yoo[34,99], J.H. Yoon[50], V. Yurchenko[3], V. Zaccolo[113,84], A. Zaman[15], C. Zampolli[34], H.J.C. Zanoli[123], N. Zardoshti[104], A. Zarochentsev[138], P. Závada[56], N. Zaviyalov[102], H. Zbroszczyk[140], M. Zhalov[89], H. Zhang[21,7], X. Zhang[7], Y. Zhang[7], C. Zhang[53], Z. Zhang[7], C. Zhao[20], N. Zhigareva[54], D. Zhou[7], Y. Zhou[84], Z. Zhou[21], H. Zhu[21,7], J. Zhu[7,116], X. Zhu[7], A. Zichichi[26,12], A. Zimmermann[96], M.B. Zimmermann[34,61], S. Zimmermann[115], G. Zinovjev[3], J. Zmeskal[115]

Affiliation notes

[i] Deceased
[ii] Also at: Georgia State University, Atlanta, Georgia, United States
[iii] Also at: Also at Department of Applied Physics, Aligarh Muslim University, Aligarh, India
[iv] Also at: M.V. Lomonosov Moscow State University, D.V. Skobeltsyn Institute of Nuclear, Physics, Moscow, Russia

Collaboration Institutes

[1]A.I. Alikhanyan National Science Laboratory (Yerevan Physics Institute) Foundation, Yerevan, Armenia
[2]Benemérita Universidad Autónoma de Puebla, Puebla, Mexico
[3]Bogolyubov Institute for Theoretical Physics, Kiev, Ukraine
[4]Bose Institute, Department of Physics and Centre for Astroparticle Physics and Space Science (CAPSS), Kolkata, India
[5]Budker Institute for Nuclear Physics, Novosibirsk, Russia
[6]California Polytechnic State University, San Luis Obispo, California, United States

[7]Central China Normal University, Wuhan, China
[8]Centre de Calcul de l'IN2P3, Villeurbanne, Lyon, France
[9]Centro de Aplicaciones Tecnológicas y Desarrollo Nuclear (CEADEN), Havana, Cuba
[10]Centro de Investigaciones Energéticas Medioambientales y Tecnológicas (CIEMAT), Madrid, Spain
[11]Centro de Investigación y de Estudios Avanzados (CINVESTAV), Mexico City and Mérida, Mexico
[12]Centro Fermi - Museo Storico della Fisica e Centro Studi e Ricerche "Enrico Fermi', Rome, Italy
[13]Chicago State University, Chicago, Illinois, United States
[14]China Institute of Atomic Energy, Beijing, China
[15]COMSATS Institute of Information Technology (CIIT), Islamabad, Pakistan
[16]Departamento de Física de Partículas and IGFAE, Universidad de Santiago de Compostela, Santiago de Compostela, Spain
[17]Department of Physics, Aligarh Muslim University, Aligarh, India
[18]Department of Physics, Ohio State University, Columbus, Ohio, United States
[19]Department of Physics, Sejong University, Seoul, South Korea
[20]Department of Physics, University of Oslo, Oslo, Norway
[21]Department of Physics and Technology, University of Bergen, Bergen, Norway
[22]Dipartimento di Fisica dell'Università 'La Sapienza' and Sezione INFN, Rome, Italy
[23]Dipartimento di Fisica dell'Università and Sezione INFN, Cagliari, Italy
[24]Dipartimento di Fisica dell'Università and Sezione INFN, Trieste, Italy
[25]Dipartimento di Fisica dell'Università and Sezione INFN, Turin, Italy
[26]Dipartimento di Fisica e Astronomia dell'Università and Sezione INFN, Bologna, Italy
[27]Dipartimento di Fisica e Astronomia dell'Università and Sezione INFN, Catania, Italy
[28]Dipartimento di Fisica e Astronomia dell'Università and Sezione INFN, Padova, Italy
[29]Dipartimento di Fisica 'E.R. Caianiello' dell'Università and Gruppo Collegato INFN, Salerno, Italy
[30]Dipartimento DISAT del Politecnico and Sezione INFN, Turin, Italy
[31]Dipartimento di Scienze e Innovazione Tecnologica dell'Università del Piemonte Orientale and INFN Sezione di Torino, Alessandria, Italy
[32]Dipartimento Interateneo di Fisica 'M. Merlin' and Sezione INFN, Bari, Italy
[33]Division of Experimental High Energy Physics, University of Lund, Lund, Sweden
[34]European Organization for Nuclear Research (CERN), Geneva, Switzerland
[35]Excellence Cluster Universe, Technische Universität München, Munich, Germany
[36]Faculty of Engineering, Bergen University College, Bergen, Norway
[37]Faculty of Mathematics, Physics and Informatics, Comenius University, Bratislava, Slovakia
[38]Faculty of Nuclear Sciences and Physical Engineering, Czech Technical University in Prague, Prague, Czech Republic
[39]Faculty of Science, P.J. Šafárik University, Košice, Slovakia
[40]Faculty of Technology, Buskerud and Vestfold University College, Tonsberg, Norway
[41]Frankfurt Institute for Advanced Studies, Johann Wolfgang Goethe-Universität Frankfurt, Frankfurt, Germany
[42]Gangneung-Wonju National University, Gangneung, South Korea
[43]Gauhati University, Department of Physics, Guwahati, India
[44]Helmholtz-Institut für Strahlen- und Kernphysik, Rheinische Friedrich-Wilhelms-Universität Bonn, Bonn, Germany
[45]Helsinki Institute of Physics (HIP), Helsinki, Finland
[46]Hiroshima University, Hiroshima, Japan
[47]Indian Institute of Technology Bombay (IIT), Mumbai, India
[48]Indian Institute of Technology Indore, Indore, India
[49]Indonesian Institute of Sciences, Jakarta, Indonesia
[50]Inha University, Incheon, South Korea
[51]Institut de Physique Nucléaire d'Orsay (IPNO), Université Paris-Sud, CNRS-IN2P3, Orsay, France
[52]Institute for Nuclear Research, Academy of Sciences, Moscow, Russia
[53]Institute for Subatomic Physics of Utrecht University, Utrecht, Netherlands
[54]Institute for Theoretical and Experimental Physics, Moscow, Russia
[55]Institute of Experimental Physics, Slovak Academy of Sciences, Košice, Slovakia
[56]Institute of Physics, Academy of Sciences of the Czech Republic, Prague, Czech Republic
[57]Institute of Physics, Bhubaneswar, India
[58]Institute of Space Science (ISS), Bucharest, Romania

[59]Institut für Informatik, Johann Wolfgang Goethe-Universität Frankfurt, Frankfurt, Germany
[60]Institut für Kernphysik, Johann Wolfgang Goethe-Universität Frankfurt, Frankfurt, Germany
[61]Institut für Kernphysik, Westfälische Wilhelms-Universität Münster, Münster, Germany
[62]Instituto de Ciencias Nucleares, Universidad Nacional Autónoma de México, Mexico City, Mexico
[63]Instituto de Física, Universidade Federal do Rio Grande do Sul (UFRGS), Porto Alegre, Brazil
[64]Instituto de Física, Universidad Nacional Autónoma de México, Mexico City, Mexico
[65]IRFU, CEA, Université Paris-Saclay, F-91191 Gif-sur-Yvette, France, Saclay, France
[66]iThemba LABS, National Research Foundation, Somerset West, South Africa
[67]Joint Institute for Nuclear Research (JINR), Dubna, Russia
[68]Konkuk University, Seoul, South Korea
[69]Korea Institute of Science and Technology Information, Daejeon, South Korea
[70]KTO Karatay University, Konya, Turkey
[71]Laboratoire de Physique Corpusculaire (LPC), Clermont Université, Université Blaise Pascal, CNRS–IN2P3, Clermont-Ferrand, France
[72]Laboratoire de Physique Subatomique et de Cosmologie, Université Grenoble-Alpes, CNRS-IN2P3, Grenoble, France
[73]Laboratori Nazionali di Frascati, INFN, Frascati, Italy
[74]Laboratori Nazionali di Legnaro, INFN, Legnaro, Italy
[75]Lawrence Berkeley National Laboratory, Berkeley, California, United States
[76]Moscow Engineering Physics Institute, Moscow, Russia
[77]Nagasaki Institute of Applied Science, Nagasaki, Japan
[78]National and Kapodistrian University of Athens, Physics Department, Athens, Greece, Athens, Greece
[79]National Centre for Nuclear Studies, Warsaw, Poland
[80]National Institute for Physics and Nuclear Engineering, Bucharest, Romania
[81]National Institute of Science Education and Research, Bhubaneswar, India
[82]National Nuclear Research Center, Baku, Azerbaijan
[83]National Research Centre Kurchatov Institute, Moscow, Russia
[84]Niels Bohr Institute, University of Copenhagen, Copenhagen, Denmark
[85]Nikhef, Nationaal instituut voor subatomaire fysica, Amsterdam, Netherlands
[86]Nuclear Physics Group, STFC Daresbury Laboratory, Daresbury, United Kingdom
[87]Nuclear Physics Institute, Academy of Sciences of the Czech Republic, Řež u Prahy, Czech Republic
[88]Oak Ridge National Laboratory, Oak Ridge, Tennessee, United States
[89]Petersburg Nuclear Physics Institute, Gatchina, Russia
[90]Physics Department, Creighton University, Omaha, Nebraska, United States
[91]Physics Department, Panjab University, Chandigarh, India
[92]Physics Department, University of Cape Town, Cape Town, South Africa
[93]Physics Department, University of Jammu, Jammu, India
[94]Physics Department, University of Rajasthan, Jaipur, India
[95]Physikalisches Institut, Eberhard Karls Universität Tübingen, Tübingen, Germany
[96]Physikalisches Institut, Ruprecht-Karls-Universität Heidelberg, Heidelberg, Germany
[97]Physik Department, Technische Universität München, Munich, Germany
[98]Purdue University, West Lafayette, Indiana, United States
[99]Pusan National University, Pusan, South Korea
[100]Research Division and ExtreMe Matter Institute EMMI, GSI Helmholtzzentrum für Schwerionenforschung GmbH, Darmstadt, Germany
[101]Rudjer Bošković Institute, Zagreb, Croatia
[102]Russian Federal Nuclear Center (VNIIEF), Sarov, Russia
[103]Saha Institute of Nuclear Physics, Kolkata, India
[104]School of Physics and Astronomy, University of Birmingham, Birmingham, United Kingdom
[105]Sección Física, Departamento de Ciencias, Pontificia Universidad Católica del Perú, Lima, Peru
[106]Sezione INFN, Bari, Italy
[107]Sezione INFN, Bologna, Italy
[108]Sezione INFN, Cagliari, Italy
[109]Sezione INFN, Catania, Italy
[110]Sezione INFN, Padova, Italy
[111]Sezione INFN, Rome, Italy

[112]Sezione INFN, Trieste, Italy
[113]Sezione INFN, Turin, Italy
[114]SSC IHEP of NRC Kurchatov institute, Protvino, Russia
[115]Stefan Meyer Institut für Subatomare Physik (SMI), Vienna, Austria
[116]SUBATECH, Ecole des Mines de Nantes, Université de Nantes, CNRS-IN2P3, Nantes, France
[117]Suranaree University of Technology, Nakhon Ratchasima, Thailand
[118]Technical University of Košice, Košice, Slovakia
[119]Technical University of Split FESB, Split, Croatia
[120]The Henryk Niewodniczanski Institute of Nuclear Physics, Polish Academy of Sciences, Cracow, Poland
[121]The University of Texas at Austin, Physics Department, Austin, Texas, United States
[122]Universidad Autónoma de Sinaloa, Culiacán, Mexico
[123]Universidade de São Paulo (USP), São Paulo, Brazil
[124]Universidade Estadual de Campinas (UNICAMP), Campinas, Brazil
[125]Universidade Federal do ABC, Santo Andre, Brazil
[126]University of Houston, Houston, Texas, United States
[127]University of Jyväskylä, Jyväskylä, Finland
[128]University of Liverpool, Liverpool, United Kingdom
[129]University of Tennessee, Knoxville, Tennessee, United States
[130]University of the Witwatersrand, Johannesburg, South Africa
[131]University of Tokyo, Tokyo, Japan
[132]University of Tsukuba, Tsukuba, Japan
[133]University of Zagreb, Zagreb, Croatia
[134]Université de Lyon, Université Lyon 1, CNRS/IN2P3, IPN-Lyon, Villeurbanne, Lyon, France
[135]Université de Strasbourg, CNRS, IPHC UMR 7178, F-67000 Strasbourg, France, Strasbourg, France
[136]Università degli Studi di Pavia, Pavia, Italy
[137]Università di Brescia, Brescia, Italy
[138]V. Fock Institute for Physics, St. Petersburg State University, St. Petersburg, Russia
[139]Variable Energy Cyclotron Centre, Kolkata, India
[140]Warsaw University of Technology, Warsaw, Poland
[141]Wayne State University, Detroit, Michigan, United States
[142]Wigner Research Centre for Physics, Hungarian Academy of Sciences, Budapest, Hungary
[143]Yale University, New Haven, Connecticut, United States
[144]Yonsei University, Seoul, South Korea
[145]Zentrum für Technologietransfer und Telekommunikation (ZTT), Fachhochschule Worms, Worms, Germany